Marine Geology 493 (2026) 107717

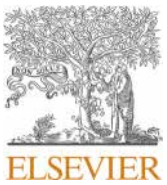

Contents lists available at ScienceDirect

Marine Geology

journal homepage: www.elsevier.com/locate/margo

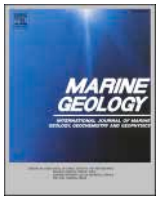

Research Article

Origin and evolution of giant comet marks along the North Atlantic Deep-Water flow on the Demerara plateau

Paul Blin [a,*], Lies Loncke [a], Xavier Durrieu De Madron [a], Sébastien Zaragosi [b], Kelly Fauquembergue [a], Swanne Gontharet [c], Ivane Pairaud [d], Pauline Dupont [e], Sandrine Caquineau [c], Bruno Charriere [a], Raphael Lagarde [a], Christophe Basile [f], Scientific Team DIADEM1

[a] University of Perpignan Via Domitia, Centre de Formation et de Recherche sur les Environnements Méditerranéens, (CEFREM), UMR 5110, 52 Avenue Paul Alduy, 66100 Perpignan, France
[b] Univ. Bordeaux, CNRS, Bordeaux INP, EPOC, UMR 5805, F-33600 Pessac, France
[c] Univ. Pierre et Marie Curie, Laboratoire d'Océanographie et du Climat: Expérimentation et Approches Numériques (LOCEAN), CNRS UMR 7159, IPSL, Case 100, 4 Place Jussieu, 75252 Paris cedex 05, France
[d] Univ. of Brest, Laboratoire d'Océanographie Physique et Spatiale, Ifremer UMR 6523 CNRS IRD Plouzané, France
[e] Univ. Brest, Geo-Ocean, Ifremer, CNRS, F-29280 Plouzané, France
[f] Univ. Grenoble Alpes, Univ. Savoie Mont Blanc, CNRS, IRD, Univ. Gustave Eiffel, ISTerre, 38000 Grenoble, France

ARTICLE INFO

Editor: Michele Rebesco

Keywords:
Comet mark
Deep western boundary current
North atlantic deep water
Deep sedimentation
Demerara plateau

ABSTRACT

The Demerara Plateau, located in the equatorial Atlantic, is particularly well-suited for recording the activity of the Deep Western Boundary Current (DWBC), which transports North Atlantic Deep Water (NADW) southward into the Atlantic basin. This current, active between 1500 and 3500 m depth, constitutes the deep part of the global thermohaline circulation and plays a crucial role in climate regulation. The Demerara Plateau is remarkable for the abundance and wide distribution of comet mark-type sedimentary structures, which can reach several kilometres in length. These hydrodynamic bedforms, interpreted as erosional features associated with strong bottom currents, are currently used as proxies for deep currents velocities, with minimum formation thresholds estimated between 0.60 and 0.75 m/s according to the literature (Rebesco et al., 2014; Werner et al., 1980). The DIADEM (Dive At DEMerara) oceanographic cruise (Basile and Loncke, 2023) enabled detailed investigation of one such structure using a combination of complementary tools with the aim of better understanding their functioning and evolution with in-situ observation, physical records, and sampling. Those new data were also combined with formerly acquired high-resolution seismic data, allowing a new vision of these bedforms their formation, and their evolution over time.

The main findings are the following: (1) comet-marks localize on carbonate mass transported blocs outcropping on the seafloor; (2) Clearly show a polyphase evolution of the bedforms of comet mark presenting alternations of erosion and sedimentation phases. The bedforms therefore record long-term variations in bottom current activity with an alternation of intense hydrodynamic events (erosion) and quieter hydrodynamic periods (deposition) through time, reflecting a complex hydrodynamic history; (3) At present, comet-marks recorded a significant decrease in current velocity within the erosional zones located inside the comet tails associated with fined-grained sediments infill in this area, highlighting the need for cautious interpretation of such features as direct indicators of present-day current intensity; (4) Finally, a result that was not necessarily anticipated but documented by exploring those bedforms with the Nautile submersible, comet-marks host quite important benthic and epibenthic biodiversity with a wide variety of associated species.

* Corresponding author.
E-mail address: paul.blin@univ-perp.fr (P. Blin).
[1] DOI : 10.17600/18000672

https://doi.org/10.1016/j.margeo.2026.107717
Received 25 September 2025; Received in revised form 15 January 2026; Accepted 20 January 2026
Available online 22 January 2026
0025-3227/© 2026 The Author(s). Published by Elsevier B.V. This is an open access article under the CC BY license (http://creativecommons.org/licenses/by/4.0/).

1. Introduction

Comet marks are erosional sedimentary bedforms typically associated with highly energetic bottom currents. In deep environments (> 200 m depth), they are mostly observed in contourite depositional systems, particularly in the North Atlantic Ocean (Kenyon, 1986; Kuijpers et al., 2002; Masson, 2001; Masson et al., 2004), and are usually used as proxies for bottom current direction and intensity. These structures are considered as "geologic current-meters" (Berton and Vesely, 2018; Masson et al., 2004; Rebesco et al., 2014) providing indirect estimations of flow direction and velocity with minimum values of 0.60–0.75 m/s (Berton and Vesely, 2018; Masson et al., 2004; Wynn and Masson, 2008). From a morphological standpoint, comet marks consist of an upstream indurated obstacle, known as the "comet head", followed downstream by an elongated erosional tail, or "comet tail". Surrounding the obstacle, a crescent-shaped erosional feature called a crescent scour may also develop. The comet head can originate from a variety of processes and materials, such as iceberg-rafted debris in polar regions (Kuijpers et al., 1993; Masson, 2001), pockmarks and methane-derived authigenic carbonates (Berton and Vesely, 2018), shipwrecks in shallow marine settings (Caston, 1979; Quinn, 2006), or mass-transport blocks in slope environments (Foglini et al., 2016). Although most comet marks have been reported in relatively shallow environments, such structures have also been identified in deep-sea settings associated with intermediate to deep-water masses such as the North Atlantic Deep-Water flow (NADW). Nevertheless, despite their apparent potential as hydrodynamic proxies, just a few comet mark fields have been studied in detail (Kuijpers et al., 2002; Kuijpers and Nielsen, 2016) in high-energy zones where near bottom currents are measured and exceed 0.6 - to >0.9 m/s corresponding to the speed required to create these structures. Laboratory flume experiments using centimetre-scale obstacles (Werner et al., 1980)demonstrated that the length of comet tails is proportional to the size of the obstacle and to the magnitude of current.

Bathymetric surveys carried out off the northeastern coast of south America over the last decade (Basile Christophe, 2016, DOI: 10.17600/16001900; Le Suave and Beuzart, 2003, DOI: 10.17600/3010050; Loncke Lies, 2013, DOI: 10.17600/13010030) allowed the identification of hundreds of giant comet marks of several kilometres in size on the Demerara Plateau. Thesedeveloped along the North Atlantic Deep-Water Flow (NADW) called the Deep Western Boundary Current (DWBC). This work focuses on one of those giant comet marks, along with a number of other comet mark, and is based on data from two oceanographic campaigns including bathymetry, reflectivity, sedimentology, seismic data, Nautile dives with direct observations of the seabed and oceanographic measurements along this bedform; IGUANES: Instabilities and fluid outflows from the Guyana-Suriname transform margin (Loncke Lies, 2013, DOI: 10.17600/13010030) and DIADEM: DIve At DEMerara (Basile and Loncke, 2023, DOI: 10.17600/18000672).

The first motivation of this study is to better understand the genesis and the past and present evolution of those giant comet marks by answering the following questions: (1) What is the origin of the indurated blocks forming the comet heads? (2) Are the comet-like structures subject to continuous erosion, or do they represent different dynamic regimes, including sedimentation-dominated phases? (3) Can giant comet marks be reliably used as "geocurrentometers" to reconstruct variations in bottom current intensity over time? (4) How do variations in sedimentary facies and bedforms along the length of the comet structures influence benthic biodiversity and faunal abundance?

Therefore, we propose (1) to synthesize available geophysical, geological and sedimentological data to propose a scenario of emplacement (2) and evolution of this comet-mark bedform, (3) to compare these observations with oceanographic measurements, (4) and finally, to describe the discovered biodiversity and discuss if this comet-mark can be considered a site with remarkable high biodiversity.

2. Study site and geological setting

The Demerara Plateau is a large bathymetric indentation prolonging the French Guiana and Suriname continental shelf (Fig. 1). It is approximately 170 km long on a South-North axis and 300 km long on an East-West axis. Most of the plateau lies at depths ranging from 500 to 4500 m.

This plateau is considered to have formed as a volcanic margin in the Jurassic, finally individualized in its actual shape in the Cretaceous after final separation between America and Africa in a transform mode (Loncke et al., 2022). Since the upper Albian, the Demerara plateau is a passive margin (Basile et al., 2013; Gouyet, 1988). Fanget et al. (2020) defined three main post-rift evolutionary stages. Firstly, a pre-contourite Stage (late Albian to early Miocene) during which sedimentation is strongly controlled by the structure of the margin and its thermal subsidence. Pattier et al. (2013a, 2013b) described during this stage several large Mass Transport Deposits (MTDs) that have been tentatively attributed to a combination of fluid overpressure and instability of the steep, transform-derived, distal plateau. Secondly, a transitional Stage (middle Miocene to early Pliocene) during which the modern thermohaline circulation establishment with the progressive closure of the Isthmus of Panama (Haug and Tiedemann, 1998). This stage is expressed by the development of a middle Miocene current-controlled erosive surface followed by the last regional mass transport deposit named « LM-EP MTD » for « Late Miocene, Early Pliocene » MTD (Pattier et al., 2013a, 2013b, synthetized in Fanget et al., 2020). Thirdly, a contouritic Stage (middle Pliocene to Holocene), characterized by the development of a contourite depositional system, identifiable mainly on the basis of systematic alternations in grain size, shifting from clay to silt intervals, linked to the circulation of the NADW, transported by the Deep Western Boundary Current.

(Tallobre et al., 2016, 2021) described in detail the recent evolution of this contourite depositional systems focusing on the contourite drift sediments that record NADW dynamics with alternating thinning and coarsening upward sequences visible on core data. Hundreds of comet-marks can be observed on the Demerara plateau's surface, between 2300 and 4200 m depth, parallel to the NADW flow (Fig. 1) as confirmed by 8 months of mooring data (Tallobre et al., 2016). Some of those comet-marks have been imaged by high resolution seismics and chirp data. The comet heads are localized above transparent acoustic highs that were tentatively proposed to be mass-transported blocks, authigenic carbonate mounds or coral mounds (Loncke et al., 2016).

3. Materials and methods

We focus in this study on one comet mark belonging to the "Tangara" field (Loncke et al., 2016) that has been imaged by IGUANES High Resolution (HR) seismic and bathymetric data in 2013 (Loncke Lies, 2013). Two additional platforms were deployed during the DIADEM campaign in 2023 to enable a more detailed and thorough analysis of these object (Basile and Loncke, 2023): (1) the IFREMER's Idef^{x}, Autonomous Underwater Vehicle (AUV), which is an uninhabited submersible diving to depths up to 2800 m and travelling around 70 m above the seabed at a speed of 1.5 m/s. Different payloads (Sub-Bottom Profiler: SBP, MultiBeam Echo Sounder: MBES, Acoustic Doppler Current Profiler: ADCP) were used during different dives. (2) The IFREMER Nautile inhabited submersible, which can dive to depths of 6000 m.

3.1. Seismic data

Four seismic profiles were used in this study: two High-Resolution (HR) seismic profiles from the IGUANES campaign, one taken along the axis of the comet (IG 53 HR) and the other across the axis (IG 40 HR), and two others based on ship-borne SBP data (IGUANES campaign) and AUV SBP data (DIADEM campaign) both aligned along the axis of the comet (IG 53 HR) (Fig. 2).

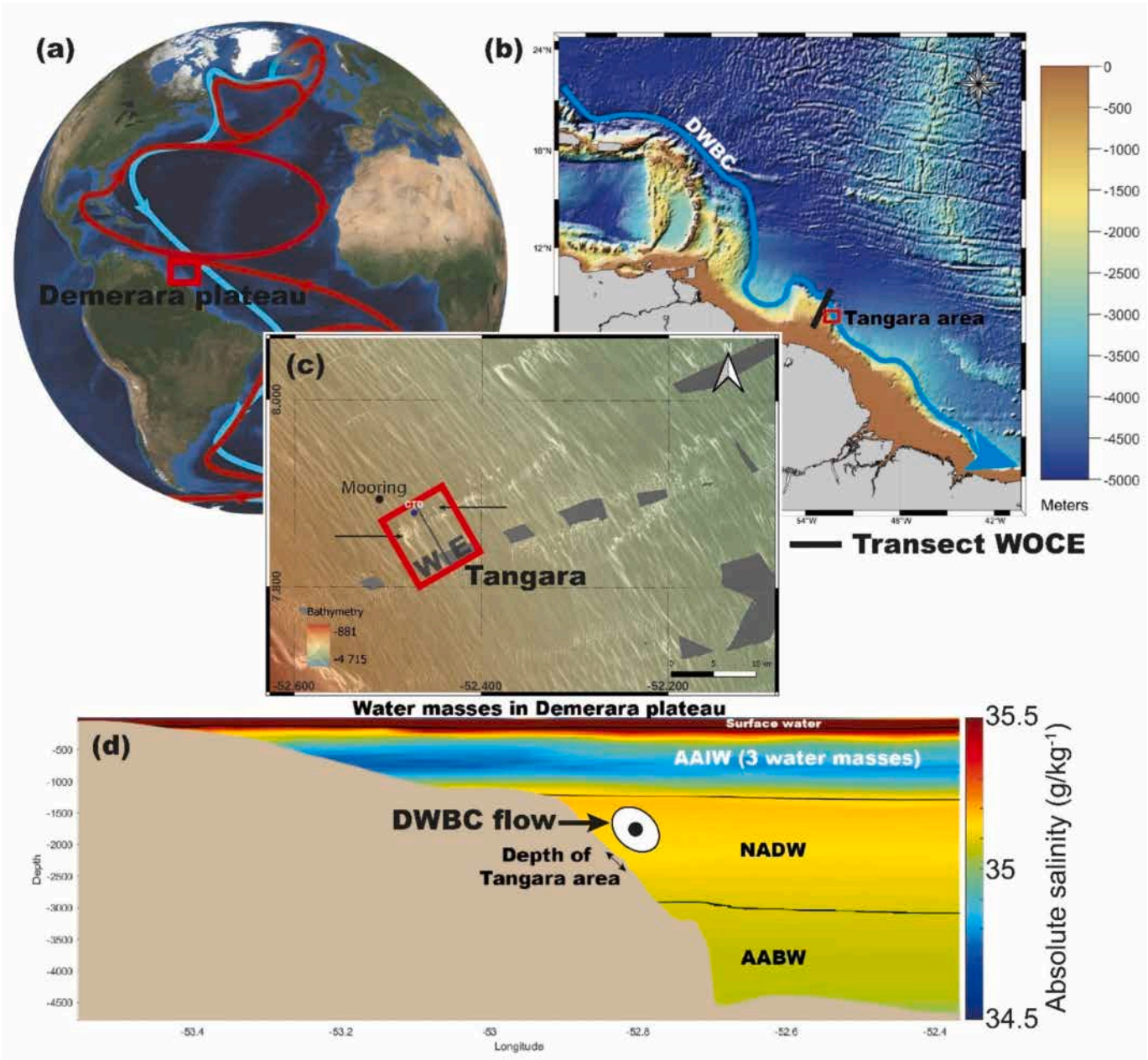

Fig. 1. (a) Position of the Demerara Plateau with the Atlantic Meridional Overturning Circulation way, with surface current represented in red and deep current in blue. (b) Regional zoom on the Demerara Plateau with pathway of Deep Western Boundary Current (DWBC) and position of the WOCE profile 16 (World Ocean Circulation Experiment, Klaus Peter Koltermann, V.G, 2011) and the Tangara region, (c) 100 m resolution bathymetry in the area of the Tangara region showing the giant comet fields, with two comet marks study here, as indicated by the two arrows. Positioning of the mooring and CTD. (d) Profile WOCE of absolute salinity transect, highlighting the four major water masses (AAIW: AntArctic Intermediate Water, AABW: AntArctic Bottom Water), the depth range of the study area and the main flow of the NADW, known as the Deep Western Boundary Current (DWBC). (For interpretation of the references to colour in this figure legend, the reader is referred to the web version of this article.)

All the seismic data from the ship were collected during the IGUANES oceanographic campaign in 2013 (Loncke Lies, 2013). Two types of seismic data from the vessel are used in this study: high-resolution seismic and chirp (Sub-Bottom Profiler: SBP), acquired simultaneously at an acquisition speed of 5 kts. The high-resolution seismic data use 72 channels and has a maximum vertical resolution of 4 m, 1 s twtt (Two Way Travel-Time) penetration. The record was processed using the IFREMER QC-Sispeed software (Loncke et al., 2016; Tallobre et al., 2016). Some key reflectors could be correlated to industrial drill data (Gouyet, 1988) and we use in this paper the correlations established by Fanget et al. (2020) and Pattier et al. (2013a, 2013b). The SBP ship data has a horizontal resolution of 20 m for a depth of 500 m and 60 m for a depth of 4000 m and 20 to 30 cm vertical resolution, 0.5 s twtt penetration. The chirp ship data were processed using the IFREMER Subop software (Loncke et al., 2016; Tallobre et al., 2016).

The data from the SBP of the AUV were collected by an ECHOES 5000 IXBlue with a frequency between 1.8 and 6.5 kHz. IFREMER SUBOP software (v3.3.2) was used to process these chirp data. The horizontal and vertical resolution of this SBP is 25 cm. A malfunction in the power electronics board altered data acquisition. In addition, large bursts of noise associated with acoustic communication with the AUV contaminated some of the pings. On average, the signal-to-noise ratio was 7 dB and the penetration varied from a few milliseconds in

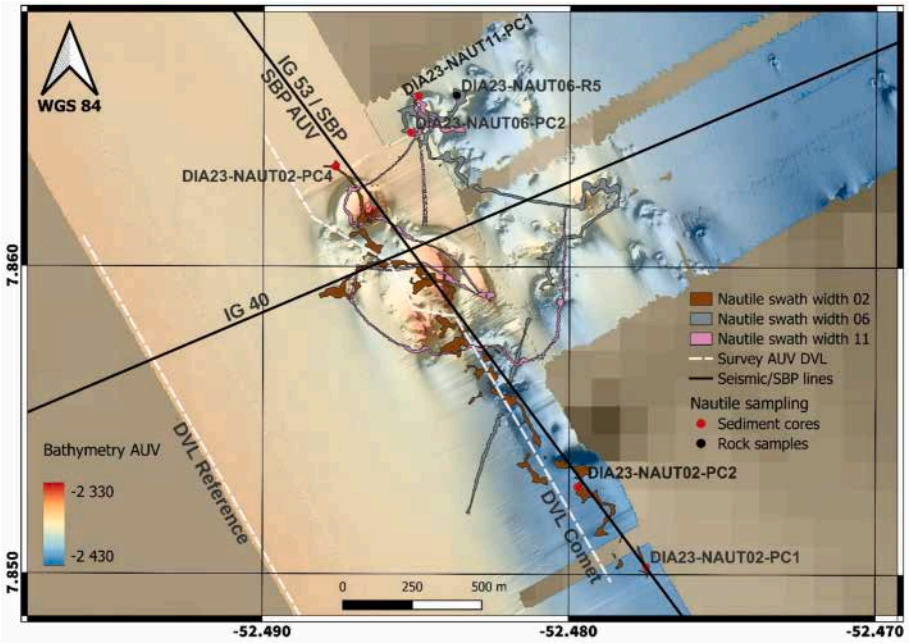

Fig. 2. Data collected on the giant Tangara comet mark including: 2 m resolution DTM from AUV (presented map), three Nautile dives (the swath width of the observations varies according to the camera parameters), sediment cores and rock samples from Nautile, seismic and sub-bottom profiler lines along and across the comet-mark and current measurements from AUV surveys.

indurated areas to more than 50 milliseconds in more sedimentary areas (Dupont and Pacault, 2023).

3.2. Bathymetric data

The multibeam echosounder (MBES) system used on the AUV in DIADEM oceanographic campaign (Basile and Loncke, 2023) utilized a Kongsberg Maritime EM2040 operating at 400 kHz for high-resolution seafloor mapping. The initial plan was to image all comet-marks of the Tangara field in its entirety. Due to bad weather conditions, all MBES dives were not completed. The focus is on the biggest one and only 80% of the comet was mapped. Fortunately, we only missed the eastern edge of the comet tail (Fig. 2).

The MBES processing unit interfaced with the AUV's attitude control unit, pressure sensor, and payload controller to ensure precise data acquisition. To prevent acoustic interference, the OSEA synchronization software coordinated transmissions between the Doppler Velocity Logger (DVL) and obstacle sounder. Bathymetric data from the MBES were processed using IFREMER's GLOBE software (Poncelet et al., 2025) to generate a Digital Terrain Model (DTM). This DTM was manually recalibrated against the ship DTM at 50 m resolution and meshed at 2 m resolution, with a sliding window of 6 × 6 grid nodes (WGS84 ellipsoid, Mercator projection). Reflectivity data were processed and recalibrated using IFREMER's SonarScope software (Augustin, 2023), while water column acoustic reflections were analyzed through the IFREMER's GLOBE software (Dupont and Blin, 2023) .

3.3. Oceanographic data

3.3.1. Moored current measurements

During the DIADEM mission (Basile and Loncke, 2023), a mooring was deployed on January 15, 2023, at coordinates 7° 53.484′N, 52° 29.898′W at a depth of 2421 m and recovered after 17.5 days. The mooring was positioned outside the Tangara comet-mark field to serve as reference not perturbed by local current accelerations associated with obstacles on the seafloor. It was equipped with two acoustic current meters, which recorded water-current velocity (speed and direction) every five minutes. A Nortek Aquadopp single-point current meter was positioned 324 m above the seabed to measure currents. Meanwhile, a downward-looking RDI WorkHorse 300 kHz current profiler was placed 63 m above the seabed to measure variation of velocities near the bottom, covering a range of 60 to 4 m above the bottom in 4 m vertical cells.

3.3.2. AUV current measurements

A 300 KHz Doppler Velocity Log (DVL), which typically serve to operate the AUV's inertial navigation system by estimating velocity relative to the seafloor, was used as a payload in water profiling mode to serve as an ADCP for velocity measurements during the two DIADEM (Basile and Loncke, 2023) AUV dives dedicated to current measurements above the bottom. The DVL was operated in slave mode with the DVL that was used for navigation purpose as a PHINS (Precise Hybrid Inertial Navigation System) inertial central input. The instrument used was a 300 kHz RDI WorkHorse Navigator (four beams at 30° beam angle), that collected velocity profiles along 14 vertical cells of 4 m size, over the last 64 m above the seafloor, every 2 s. The acquisition methodology using VMDAS for merging of ADCP and navigation data, and the data processing, are based on the method described in Pairaud and Fuchs (2021). Post-processing of DVL velocity data required a specialized workflow distinct from standard ADCP data processing. This involves considering the magnetic deviation depending on where the compass calibration was performed, and integrating navigation parameters (AUV position, speed relative to the seafloor, and heading) and attitude data (roll and pitch) from the inertial central (considering the lever arm) to calculate horizontal velocity components in a terrestrial reference frame from ADCP raw along beam data. As the AUV was very stable and well balanced, the influence of pitch and roll was found to be negligible. Quality control was applied, particularly on correlation and signal intensity, ensuring only high-quality data were retained. Due to topographical accidents and acoustic interferences, in addition to side lobe contamination at the bottom (concerning 13% of water depth), up to five cells above the bottom (i.e. about 20 m) may be missing or corrupted and were discarded during data post-processing. For data visualization, a first median filter with a window size of 3 was applied to the U and V velocity components. Subsequently, the same median filter, with a window size of 5, was applied to the derived velocity magnitude.

3.3.3. AUV hydrological measurements

The AUV was also equipped with an SBE 49 FastCAT CTD (Conductivity, Temperature, Depth) sensor, which measures temperature, conductivity, and pressure, and derives salinity and depth from these data. The profile is formed by the measurements acquired during the spiral descent of the AUV in the water column to its operational depth 70 m above the seabed. Outliers and pressure inversions were removed during the data post-processing. The dive considered here is in the immediate vicinity of the comet head and its position was 7°52.890′N, 52°28.140′W. Derived parameters that include conservative temperature (CT) in degree Celsius, Absolute Salinity (AS) in g/kg^{-1}, and potential density anomaly referenced to 2000 dbar (σ_2) in kg/m^3 were calculated using the TEOS-10 toolbox (McDougall et al., 2011).

3.4. Nautile Submersible dives

Three different Nautile dives were carried out to visit the comet allowing visual observations as well as sediment and rock sampling (Fig. 2).

3.4.1. Positioning and photography

Nautile uses two simultaneous positioning methods for navigation. The first method combines an Inertial Navigation System (INS, Phins Surface IXblue) with a Long Baseline (USBL, Ramses IXBlue), using position, heading, speed and depth data to provide a local reference with decametric to hectometric accuracy. The second method uses an Ultra-Short Baseline (USBL, Posidonia 2 IXBlue) that integrates the GNSS position of the support vessel with vertical and horizontal triangulation to position the submersible. This approach also achieves metric to decametric accuracy for the depth of the survey site and provides a real geographical reference. To maintain accuracy, the INS drift is corrected every 15 min using the USBL system.

The Nautile is equipped with two continuously recording cameras in high definition and including one camera 4 K and three portholes for direct observation. One camera records vertically, while the main camera has two axes of movement. All motion data recorded have a frequency of 1 Hz and are synchronized.

Morphosedimentary facies on the seafloor, as well as ecological observations, are analyzed directly from the primary video recordings, with all data integrated into a GIS for interpretation. Photogrammetry was also performed using the main camera, which operates in HD quality (1080p) and is equipped with its own inertial navigation system (INS). The camera's pan and tilt are fixed relative to the Nautile's roll, pitch, and yaw values, allowing the geographic position and angle of the lens to be determined for each image (Coudun et al., 2025). The workflow is similar to terrestrial UAV (unmanned aerial vehicle) photogrammetry (Bemis et al., 2014). Frames are extracted from video using the ffmpeg software, and 3D models are created with Agisoft Metashape. The process involves aligning photos (automatically or manually), removing alignment errors exceeding 1°, cleaning outlier points in two stages, generating a point cloud, building a mesh and texture from the cloud, creating a digital terrain model (DTM) and orthomosaic from the mesh and texture, and exporting the DTM, orthomosaic, and 3D model in WGS84 UTM22N coordinates. The average percentage of distance measurements is low at 5% and does not affect the result for the bedding. For interpreting the 3D textured model, the Virtual Reality Geological Studio software was used. Bedding measurements, including strike and dip of stratigraphic surfaces and faults, are performed using VRGS's integrated bedding tool.

3.4.2. Sampling

During Nautile dives, Five push cores were also collected: two from the comet tail of the main comet-mark, one upstream of the same comet-mark, and two from crescent scours associated with smaller comet-marks surrounding the main feature, to qualify the sediment type and its variation from up to downstream (Fig. 2). Those push-cores allow to collect at maximum the first 30 cm of sediments with an excellent preservation of the water-sediment interface. Those push-cores have been split, photographed, and visually described.

Several rock samples were collected especially along comet-heads and only one is included in this study. After realizing a macroscopic description of carbonate rocks on board, these samples were frozen at −20 °C and freeze-dried until further observations. Sub-samples were finely crushed and the same "bulk" powder was used for determining the total carbonate content and identifying the mineralogical composition by X-Ray Diffraction (XRD). The total carbonate content (in wt%) was measured by reaction of 100 mg of fine powdered bulk sample with 0.4 cm^3 of HCl 8 N with an absolute error of 1%. Mineralogical identification by XRD was done on unoriented preparations analyzed by an X'Pert Powder diffractometer (PANalytical) with a Ni-filtered Cu K_α, operating at 40 kV and 40 mA (ALYSES analytic platform affiliated to Ecce Terra Observatory for Sciences of the Universe). The sample was scanned from 2 to 70° (2θ) in steps of 0.02. The identification of the major minerals was performed by comparison with referencing data from the Inorganic Crystal Structure Database (ICSD) and the Crystallography Open Database (COD) using the HighScore software (PANalytical, 3.0.5, 2012). Semi-quantitative estimation of the different minerals was obtained using the peak area in combination with total carbonate content (Gontharet et al., 2007). For this estimation, the relative error was roughly estimated at ±5%. The morphology, microstructure and elemental composition of an uncrushed carbonate rock fragment were examined with a Zeiss EVO LS15 Scanning Electron Microscope (SEM) operating at 15 kV, coupled with an INCA Energy 350 EDS microprobe (Oxford Instruments, ALYSES analytic platform affiliated to Ecce Terra Observatory for Sciences of the Universe).

Benthic community diversity was quantified using the Shannon diversity index and the Simpson index. The Shannon index is sensitive to species richness and gives greater weight to rare species, whereas the Simpson index emphasizes dominant species and community evenness (Magurran, 2004).

4. Results

4.1. Bathymetry and reflectivity

The acquired bathymetry gives a new and accurate vision of part of the Western "Tangara" comet field (Fig. 2). It is made of one complex main comet-mark, composed of multiple comet heads and crescent scour complexes associated with one elongated tail to the west. This structure is highly contrasting with the nearby undisturbed seafloor. To the east, several smaller comets are visible. They are all characterized by a comet head that is made of one to several positive reliefs surrounded by crescent scours. The comet heads range from metres to hundreds of metres in horizontal scale size and extend from meter to several tens of metres in the vertical. "Comet tails" are elongated depressions downstream of the comet-heads. The width-to-length ratio of the main comet-mark studied here is 15 (3000 m / 200 m). In the comet tail, the maximum scouring value is 64 m (depth difference between the most scoured part and the surrounding area). The reflectivity values derived from MBES data highlight distinct contrasts between comet head, tail and crescent scours (Fig. 3.a). Fig. 3.b provides a close-up view of a comet head located in the eastern Tangara area, located 4.5 km to the north-west of the study area, at depth of 2600 m (bathymetry in Fig. 6.b). The comet head exhibits the strongest reflectivity signal, forming a clear high-reflectivity patch at the obstacle. Around, the crescent scour is characterized by high reflectivity values, forming a transitional zone between the head and the tail. Finally, the comet tail shows uniformly low reflectivity, with values significantly reduced compared to the upstream sectors. This progressive decrease from the head to the tail is consistently observed along the mapped area.

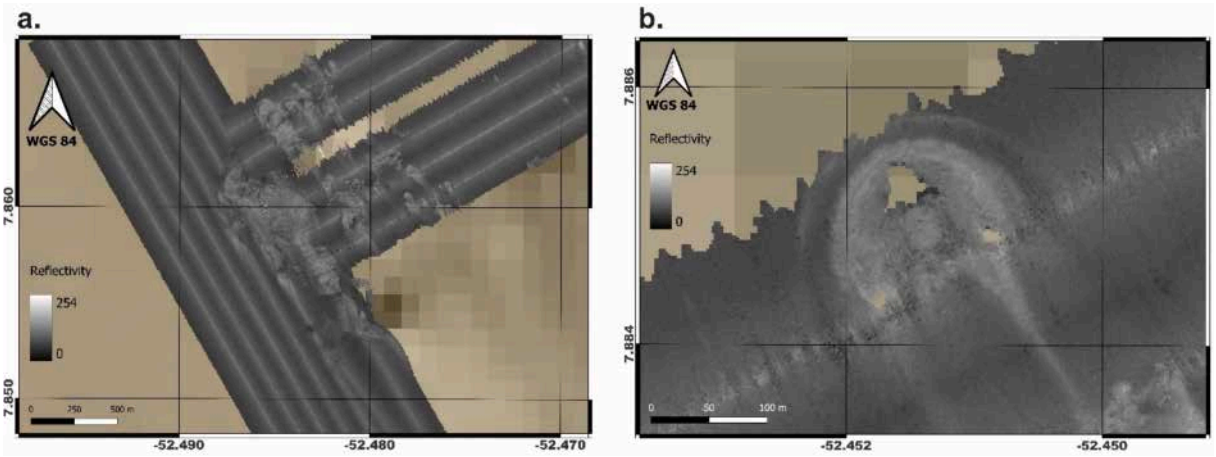

Fig. 3. Reflectivity data acquired from the AUV MBES. (a) Overview of the study area, and (b) zoom of a comet mark located in the eastern Tangara area.

4.2. Seismic analysis

Two perpendicular high-resolution seismic lines allow to image the biggest Tangara comet mark in depth. The penetration, more than 1000 ms twtt, allows to image stratigraphy up to the Albian unconformity (R6, in purple, Fig. 4). A first general observation is that the Tangara comet marks are localized on top of an acoustically transparent to chaotic mass that erodes older sediments, and that outcrops on the seafloor (coloured in blue on Fig. 4). This chaotic mass was already defined before this study as "LM/EP MTD" by Fanget et al. (2020). This LM/EP MTD is the beginning of the contourite evolutionary stage defined by the same authors. Under this mass, Albian to Cretaceous sediments are cut by numerous vertical discontinuities interpreted as faults possibly driving fluids (Pattier et al., 2013a, 2013b; Pattier et al., 2015). All faults end at the base of the LM/EP MTD.

This mass shows complex internal arrangements that evolve from upslope to downslope. Upslope, this chaotic mass has an average thickness of ~50 ms twtt (Fig. 4.c). Going downslope, where the unit outcrops, this chaotic body becomes thicker. Oblique and distorted reflectors looking like thrusts and compressive bulges appear (Fig. 4.d, in black). Internal unconformities are also visible within this complex body. The thickness of the associated chaotic body is more than doubled (~ 100 ms twtt) under the comet-marks area. Downslope of this domain, it seems like the LM-EP MTD splits into two distinct parts separated by a linear reflector called MTD2 and MTD3 respectively(Fig. 4.d – reflector underlined in grey). This reflector seems also affected by thrust faults. On the profile parallel to the slope(Figs. 4.a and 4.b), the LM-EP MTD also shows a drastic change under the comet field: numerous oblique high energy reflectors appear and if this acoustic body still corresponds to the LM-EP MTD, its thickness has more than doubled. Above this mass, the post-Pliocene sedimentation globally thins from upslope (> 100 ms twtt) to downslope (30 ms twtt) (Fig. 4.c). The Comet-field domain appears to be a low sedimented area with thickness around 22 ms twtt.

In detail, three main erosional surfaces (red, orange and yellow in Fig. 4) are visible in the post-Pliocene unit. The erosion seems to be amplified downstream, in the comet-tail. The three surfaces are deeper downstream than upstream. At the scale of the seismic data, there are no recent erosional phases recorded after the red erosional surface 03. Instead, fan-shaped sediment infills appear in the comet-tail (Fig. 4.b).

On those profiles, only the last erosional surface that was identified at the scale of high resolution seismics (erosion 03, in red Fig. 5) could be imaged. It appears as a strong reflector enclosing acoustic bodies that appear transparent due to the resolution constraints of CHIRP data. This reflector could only be observed upstream of the giant comet-head. In the comet tail it was probably too deep to be imaged. This erosion surface is covered by a first bedded but quite transparent seismic unit. Above this unit seismic amplitudes become stronger. Within this high amplitude bedded unit, two regional reflectors 00 and 01 could be picked-out and followed. Upstream of the comet-head no major evident erosional surface could be depicted but reflectors are not always strictly parallel, and sedimentary units show thickness variations. In this proximal part of the comet tail, reflectors show a clear fan-shaped arrangement, with sediment thicknesses growing in comet tail (Fig. 5.c). On AUV SBP, less prone to develop diffraction hyperbolas, the comet head is characterized by a very disrupted high amplitude reflector on the seafloor. In the comet tail, reflectors show a clear fan-shaped arrangement.

4.3. Morpho-sedimentary analysis from Nautile dives

The giant Tangara complex comet-mark imaged in Figs. 4 and 5 and some of its smaller neighbours were visited by three Nautile submersible dives (Fig. 2, Fig. 6) allowing to image and sample the different sediments or outcropping rocks. The seafloor facies are categorized into two main groups that we mapped along dive tracks (Fig. 6): rock and sedimentary facies. The rocky facies are further divided into five subtypes, all of which consist of carbonate material and are all located at comet heads:

- (1.a) Massive stratified blocks (light green): Indurated blocks with clear stratification (> 1 m);
- (1.b) Chaotic blocks (dark green): Lot of small centimetric-size reworked blocks;
- (1.c) Stratified slabs (dark blue): Indurated slabs showing stratification (< 1 m) and partly covered by fine-grained sediments;
- (1.d) Carbonate and sediments (light blue): Indurated sub-horizontal pieces of slabs covered by sediments without visible stratification;
- (1.e) Carbonate (Purple): Same as subtype facies (1.d) but without sedimentary layers.

The sedimentary facies are subdivided in six facies and are distributed across the comet tail (2.a) or the crescent scour that develops around comet heads (all other facies):

- (2.a) Bioturbated mud (Yellow): very fine mud with a lot of bioturbation mainly resulting from the activity of Echinoderms, predominant in these facies.
- (2.b) Bioturbated mud and clasts (Red): Same as facies (2.a) with a sparse clast, maybe associated with black organic-rich sediment.
- (2.c) Bioturbated mud and shells (Orange): This facies is the same as facies (2.a) but with a lot of centimetric- to metric-sized patches of shells, mostly from Gastropods, for some of them clearly fragmented.

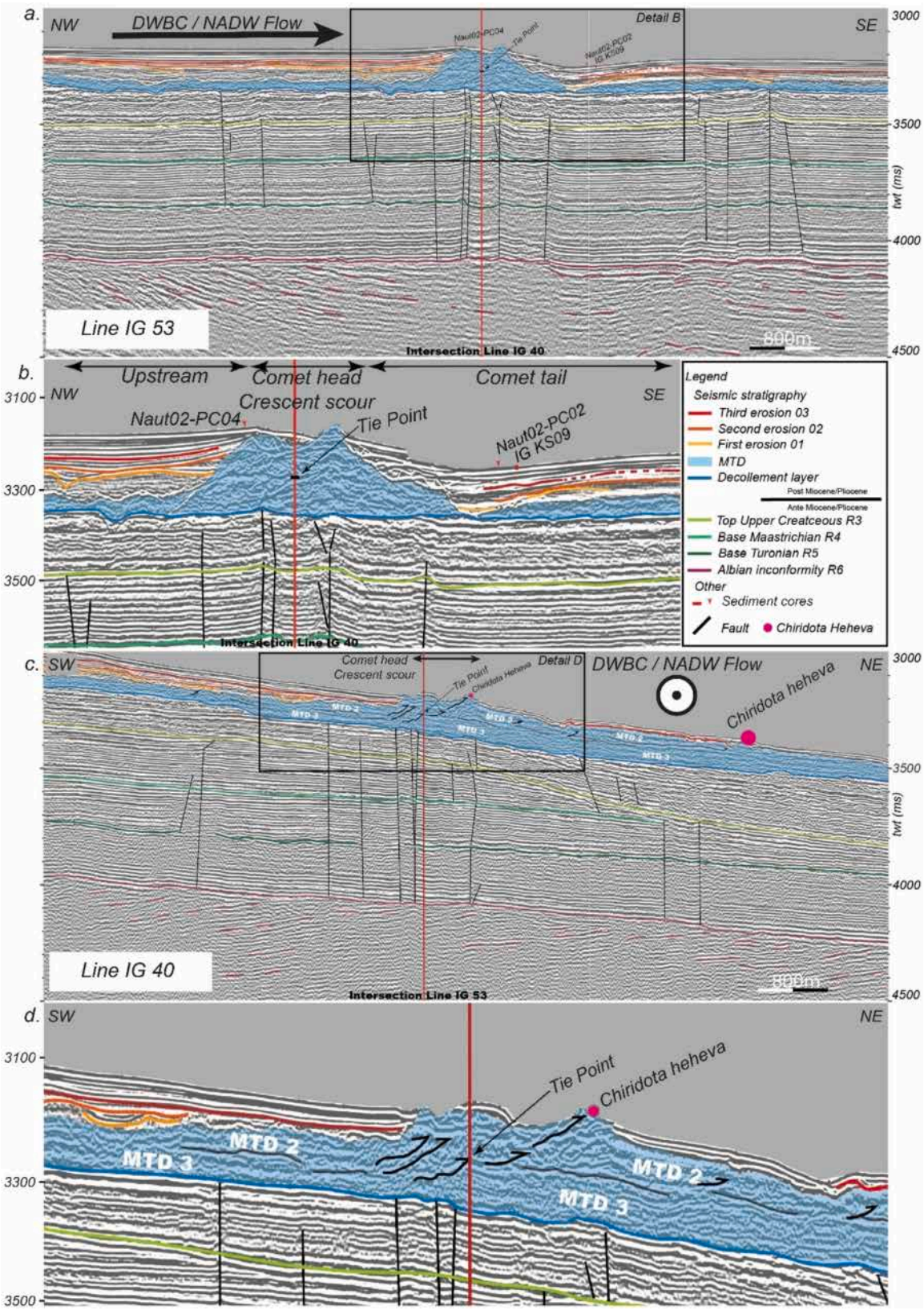

Fig. 4. High resolution seismic profiles centred on the comet area. (a.) Seismic line IG53 HR imaging the giant comet-mark in a direction parallel to the NADW flow (b.) zoom on the giant comet-mark. (c.) Seismic line IG40 HR imaging the general upslope to downslope sedimentary pattern, perpendicular to the NADW flow (d.) zoom on the study area. Naut 02 PC02 and PC04 are two 30 cm long push-cores described in this study (Fig. 9). IG-KS-09 is a 3.2 m long gravity core described by Tallobre (2017) made mainly of alternating clays, and very fine sands.

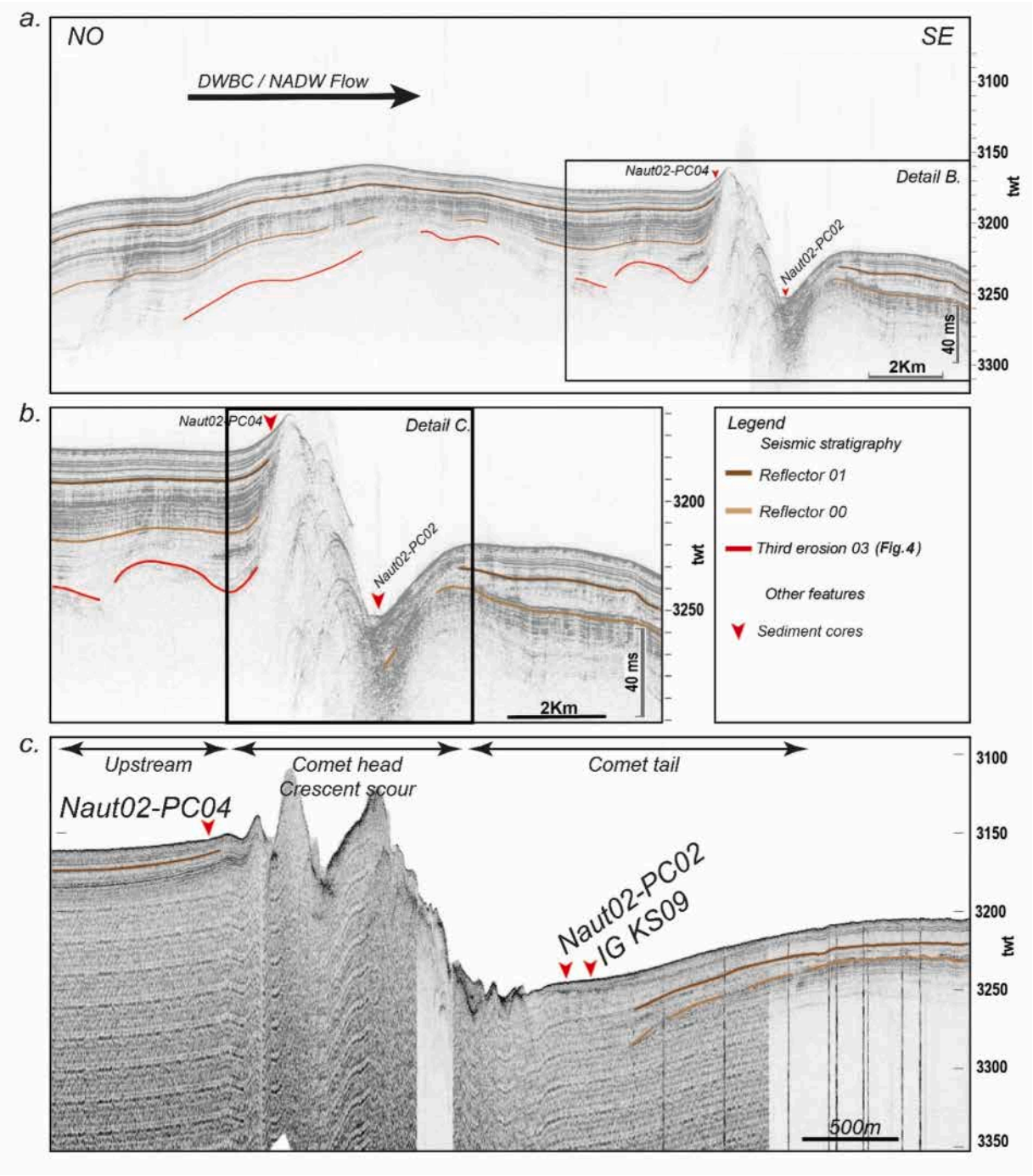

Fig. 5. Chirp seismic profiles centred on the studied giant comet-mark. (a.) SBP from vessel parallel to NADW flow and same transect to IG53 HR shown in Fig. 4.a (b.) and zoom. (c.) SBP data from AUV parallel to NADW flow and same transect to IG53 HR. Naut02-PC02 and Naut05-PC04 are two 24 cm long push-cores described in this study (Fig. 9). IG-KS-09 is a 3.2 m long gravity core described by Tallobre (2017) made mainly of alternating clays, and very fine sands.

- (2.d) Black sediments and shells (Grey): Fine black sediments probably organic-rich with a lot of shells from mostly Gastropods, distributed in patches, for some of them clearly fragmented.
- (2.e) Ripples and shells (Brown): same as facies (2.f) with homogeneous distribution of shells or shell fragments.
- (2.f) Ripples (Pink): fine silt with sedimentary current features (centimetric size and frequency)

Following the bathymetric survey and the Nautile dive, one of the first notable observations was the morphological complexity of the comets, which may consist of multiple smaller comet marks clustered around larger comet marks (Fig. 6).

Geographical distribution of facies is illustrated in Fig. 6. All comet-heads forming the obstacles around which the DWBC flows, are made of indurated carbonate rocks (facies 1.a to 1.e). The comet tail and domains surrounding the comet-mark bedforms are primarily composed of very fine bioturbated mud (Facies 2.a). Moving up from the comet tail towards the indurated areas, very heterogeneous zones appear characterized by a facies composed of bioturbated mud and containing small clasts and some patches of black - probably organic-rich - sediments (Facies 2.b). The crescent scours are composed, in their most lateral parts, of silty sediment, shells and sedimentary ripples (Facies 2.e). The

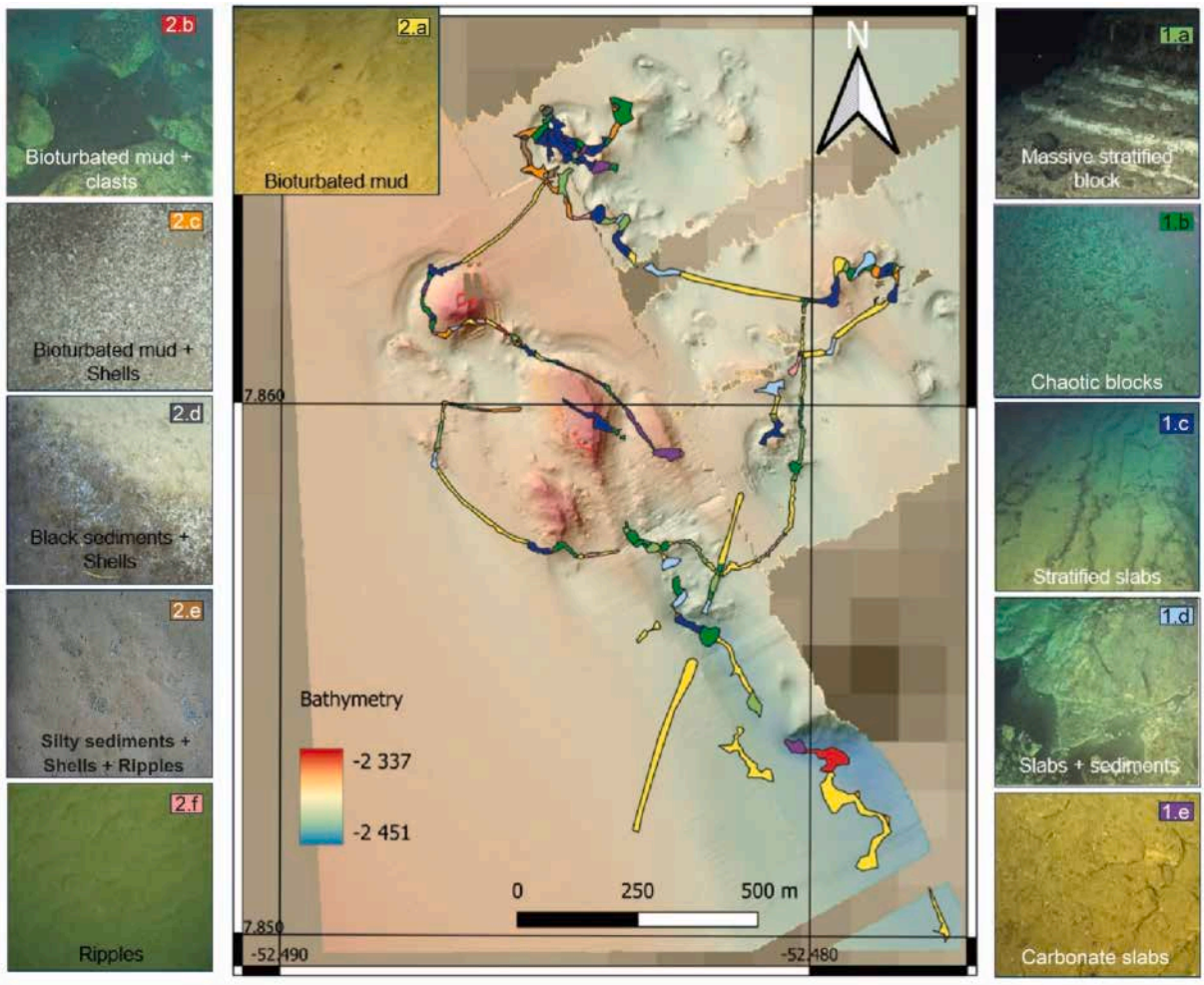

Fig. 6. 2 m resolution shaded bathymetry with Nautile dive routes. Each colour refers to facies observed on the seafloor (the swath width of the observations varies according to the camera parameters). Legend at the right correspond to the comet head facies, the left is associated with the crescent scour and comet tail domains.

front of the crescent scours is dominated by bioturbated mud with abundant shell fragments (Facies 2.c).

The comet heads are all made of carbonate rocks. The upstream part of the blocks forming the comet heads shows no sedimentation and consists mainly of stratified carbonate slabs (Facies 1.a or 1.c). The downstream part of blocks forming the comet heads are more sedimented (Facies 1.d). Reworked chaotic carbonate blocks are found all around the comet head (Facies 1.b).

4.4. Structural analysis

Structural analysis based on the 3D blocks constructed by photogrammetry (Fig. 7.a, Fig. 7.b) highlights the chaotic character of the dip values of carbonate beds throughout the Tangara area. In Tangara West, the maximum dip value is 86°, while in Tangara East it is 77°, indicating sometimes nearly vertical blocks (Fig. 7.c). More horizontal blocks are also present, with dips of 8° for Tangara West and 9° for Tangara East. The orientation of the blocks shows no recurring trend. Additionally, many of the observed blocks are faulted (Fig. 7.e), and sometimes folded (Fig. 7.d).

4.5. Petrography, geochemistry and sedimentology

The Nautile dives have enabled recovery of various fragments of carbonate outcrops. They are white when freshly broken and highly friable. A detailed analysis of the rock DIA23-Naut06-R5 located 500 m north-east of the main comet (Fig. 2) was studied.

This beige to ochre clast was collected in a scour behind a comet head found in contact with black sediments (Fig. 8.a, equivalent to Facies 2.b in Fig. 6). Its upper surface is porous, coated by a dark yellow to dark brown oxide layer (Fig. 8.b) and colonized by the deep-sea holothurian *Chiridota heheva* (Fig. 12.e). This bulk sample is mainly composed of carbonates (80.4 wt%) associated with detrital minerals (Kaolinite and illite clay (19.1 wt%) and quartz (0.1 wt%)). Detrital minerals especially occur at the surface of this rock and as a pore-filling material. Stoichiometric calcite, characterized by a $d(104)$ value of 3.035 Å, represent the only carbonate phase observed in this sample, mostly originated from pelagic or detrital sediment. SEM observations revealed that this carbonate rock was formed by numerous biogenic components of pelagic sediments embedded in clay matrix. Biogenic components mostly originate from coccoliths and planktonic foraminifera and scarce benthic foraminifera (Fig. 8.c, Fig. 8.d, Fig. 8.e). These components were generally coated by clays and numerous tests of planktonic foraminifera showed small calcite crystal aggregates resulting from recrystallisation processes (Fig. 8.d). Thin needle-like crystals of calcium carbonate, most probably composed of aragonite,with up to 10 μm in length were precipitated in a cavity and in association with a few coccoliths (Fig. 8.f).

In addition to rock samples, 5 push-cores were collected in the Tangara comet-mark field. A synthetic log descriptions of those five sediment cores (Fig. 9) are presented according to their emplacement in comet-marks: One core was collected upstream of the main Tangara

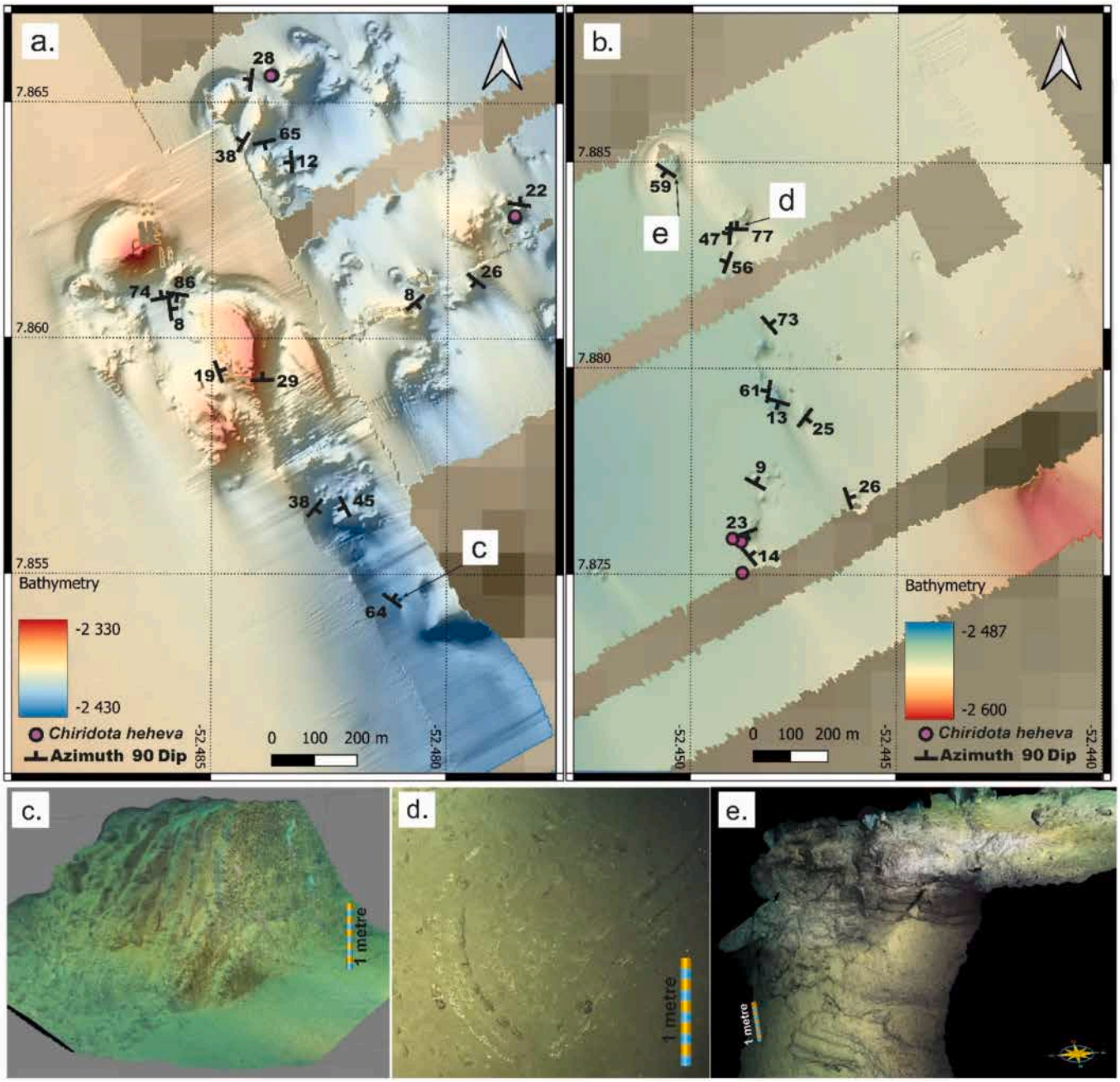

Fig. 7. Structural analysis of geological outcrops from 3D photogrammetry. (a.) Study area with measured dips. (b.) dip measurements made eastwards from the main study area on comet-marks emplaced on the lateral continuity of LM-EP MTD (Fig. 3.c). (c.) 3D block draped with camera image showing a 3 m high stratified block and notice the 64° dip. (d.) Example of small fold (thickness: 1.8 m) observed in a comet-head domain (e.) Example of 3D block showing stratified faulted carbonates.

comet: Dia23-Naut02-PC04 (collected in facies 2.a, Fig. 6). Two were collected in crescent scours domains: Dia23-Naut06-PC02 (collected in facies 2.e, Fig. 6) and DIA23-Naut11-PC01 (collected in facies 2.c, Fig. 6). Two others in the comet tail domain: DIA23-Naut02-PC01 (collected in facies 2.a, Fig. 6) and DIA23-Naut02-PC02 (collected in facies 2.a, Fig. 6). Synthetic logs of these five sediment cores are presented in Fig. 9. For DIA23-Naut02-PC01, the sediment texture ranges from fine (silt) to very fine (clay) with two slightly coarser zones identified at depths of 6 cm and 11 cm. DIA23-Naut02-PC02 shows surface sediments (0-7 cm) containing coarser sediments due to shell fragments, but sediment grain size decreases from the surface to a depth of 15 cm, eventually stabilizing as very fine sediment (Clay). DIA23-Naut11-PC01 presents sedimentation with fine sands at the surface becoming finer to silty clay. DIA23-Naut06-PC02 reveals surface sediments are fine (silty clay), with a sandy layer at 5.5 cm depth. From the surface to 13 cm depth, the sediment size remains stable before increasing to rougher sandy granulometry. DIA23-Naut02-PC04 is composed of fine (silt) surface sediments decreasing in size until 12.5 cm depth, where they are very fine sediments with occasional coarser episodes.

4.6. Oceanography

The high-resolution profiles from the AUV-mounted CTD, although stopped at its operational altitude of 70 m above the seafloor, provided coherent temperature, salinity and density structures within the bottom mixed layer (BML), as shown in Fig. 10. The BML thickness was

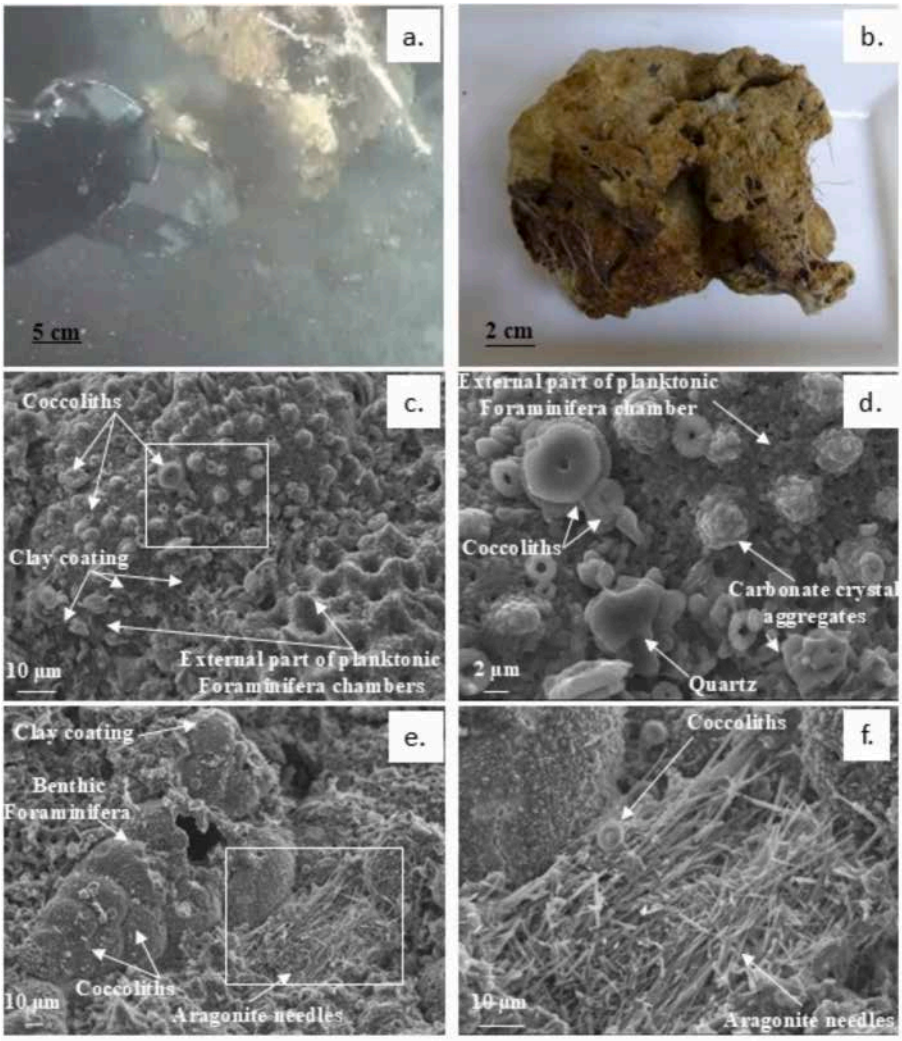

Fig. 8. a. Rock DIA23-NAUT06-R5 collected during Nautile dive 06 (Fig. 2). b. Macroscopic structure of the rock DIA23-NAUT06-R5. SEM photographs of rock DIA23-NAUT06–05 (secondary electrons) c. External part of planktonic Foraminifera chambers sometimes associated with coccoliths and scarce clay materials at their surface. d. Zoom of the 8.c photograph (white rectangle),carbonate crystal aggregates resulting from recrystallization processes affecting foraminifer tests. e. Benthic foraminifera covered by clay material and coccoliths. f. Zoom of the 8.e photograph (white rectangle) showing authigenic needle-like crystals of calcium carbonate in a small cavity.

determined using a density-difference criterion relative to the bottom-most measurement ($\Delta\sigma_2 \approx 0.005$ kg·m^{-3}), with density serving as a variable that integrates the temperature and salinity fields. Based on this approach, the BML thickness (Fig. 10) was estimated to be 156 m, while across all observed profiles the BML thickness varied between 100 and 180 m, with a median value of 120 m. The thickness of these BML greatly exceeds values from energetic Atlantic regions catalogued by (Huang et al., 2019), with a median thickness of 40 m and a 90th percentile of 100 m, suggesting enhanced interaction of the overlying DWBC with the bottom over the study area.

Mooring observations reveal depth-dependent current dynamics (Fig. 11). The upper current-meter (324 m above the seafloor) recorded semi-diurnally modulated flow already observed during the IGUANES campaign (Tallobre et al., 2016) directed almost along the isobath (147° orientation) with a mean velocity of 16.3 cm/s, showing tidal variability (6 to 28 cm/s; Fig. 11.c). In contrast, the lower acoustic profiler (4–60 m above the seafloor and within the BML) detected weaker currents (9.7 cm/s on average), deviated to the left compared to the flow of the upper layer (Fig. 11.b). This velocity reduction and leftward deflection is consistent with theoretical bottom Ekman transport expectations (Cushman-Roisin and Beckers, 2011), where bottom friction induces a cross-isobath flow component. Tidal modulation persisted in the BML, with currents along the isobath oscillating between 0 and 25 cm/s (Fig. 11.c).

A 23 min AUV transect along the comet's axis during peak tidal flow (Fig. 12) revealed clear topographic steering effects. Maximum instantaneous flow velocities from peak tidal flow for all depth (Fig. 12.a) increased approximately from 20 cm/s upstream to 44.5 cm/s at the comet's head, before gradually slowing down downstream to 14.75 cm/s at the comet's tail. For average flow velocities during this period for the different area, they remained stable between approximately 13.5 cm/s upstream and 13 cm/s at the comet's head, before gradually slowing downstream to reach 7 cm/s at the comet's tail. Upstream of the comet, currents were relatively homogeneous and aligned with the isobaths (Fig. 12.b). However, abrupt deviations of up to ±50° were observed where the steep relief of the crescent scour and the head of the comet disrupted the flow. To a lesser extent, deviations also occurred on the downstream of the comet head. Downstream of the comet, currents progressively reoriented along the axis of the comet.

4.7. Ecology

The study analyzed ecological patterns along a straight transect linking the upstream and comet tail (Fig. 13) for the Nautile swath width

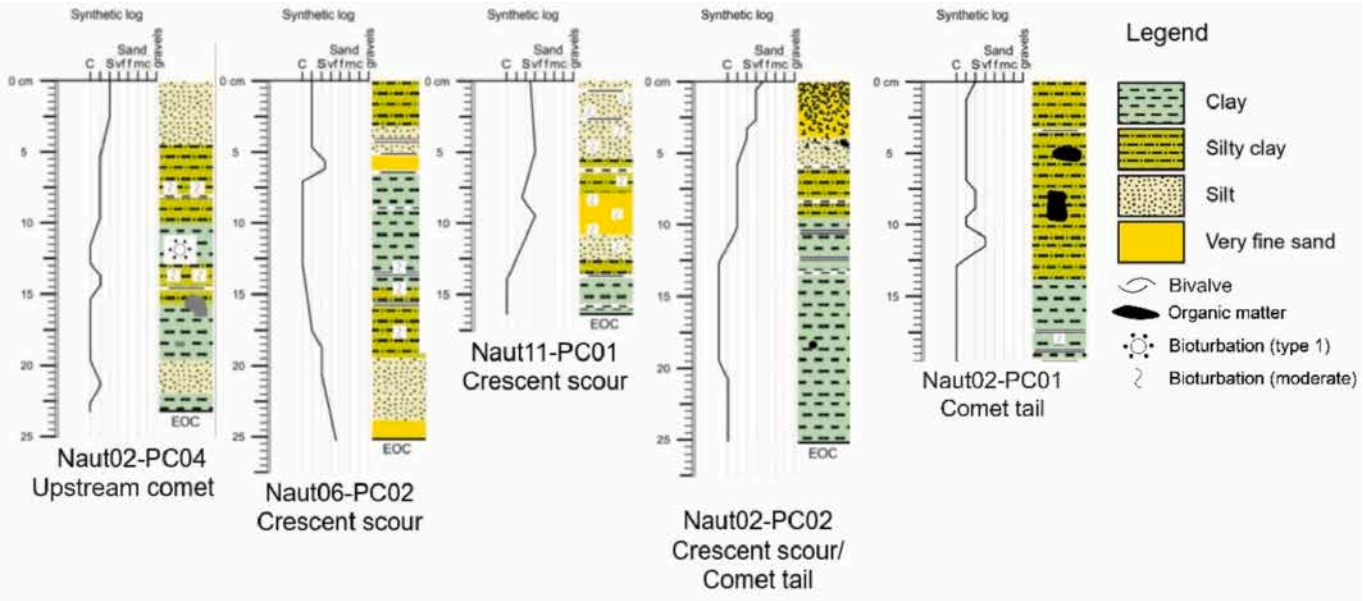

Fig. 9. Synthetic logs of Nautile push cores collected in the Tangara comet-mark field. Position of the cores is represented in Fig. 2.

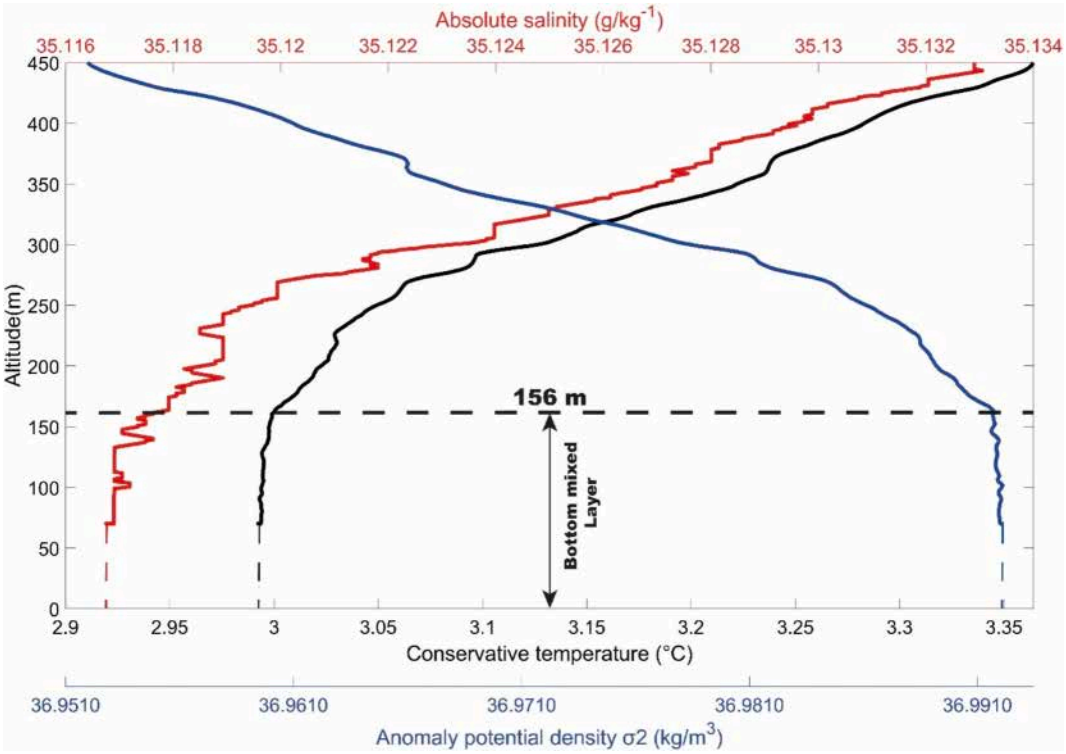

Fig. 10. Absolute salinity (red), conservative temperature (black), and potential density anomaly (blue) for the AUV dive on 19 January 2023 in the proximity of the main comet head. The profile stops at 70 m above bottom. The profiles of the BML for the different parameters have been extrapolated to the bottom. (For interpretation of the references to colour in this figure legend, the reader is referred to the web version of this article.)

02 (Fig. 2), divided into seventeen 100-m segments with manual counting to assess individual density and taxonomic diversity per unit area, with results averaged across sampled zones. Transects of 100 m length were selected to provide a sufficiently representative basis for species counts. However, this choice introduces uncertainty regarding the detection and characterization of smaller-scale structures. Fig. 13 integrates these findings with bathymetric data, comparing three distinct regions: the upstream, comet head/crescent scour, and comet tail. In total, the dive covered a total area of 47,915 m^2 in which 3434 individuals belonging to 38 different species were recorded. The five more abundant taxa are *Ophionotus victoriae, Ophiuroidea* (59% of the total individuals recorded during the dive), *Pachastrella monilifera, Demospongiae* (13.5%), *Pachastrella abyssi, Demospongiae* (8.5%), *Benthodytes lingua, Holothuroidea* (4%), and *Chrysogorgia* sp., *Octocorallia* (3.5%). The comet head and the crescent scour are not clearly distinguishable here due to the complexity of the area and the heterogeneity of the facies. The comet tail without blocks on the seafloor (3 last segments) exhibit notably low taxonomic diversity (0.9 taxon per 1000 m^2),

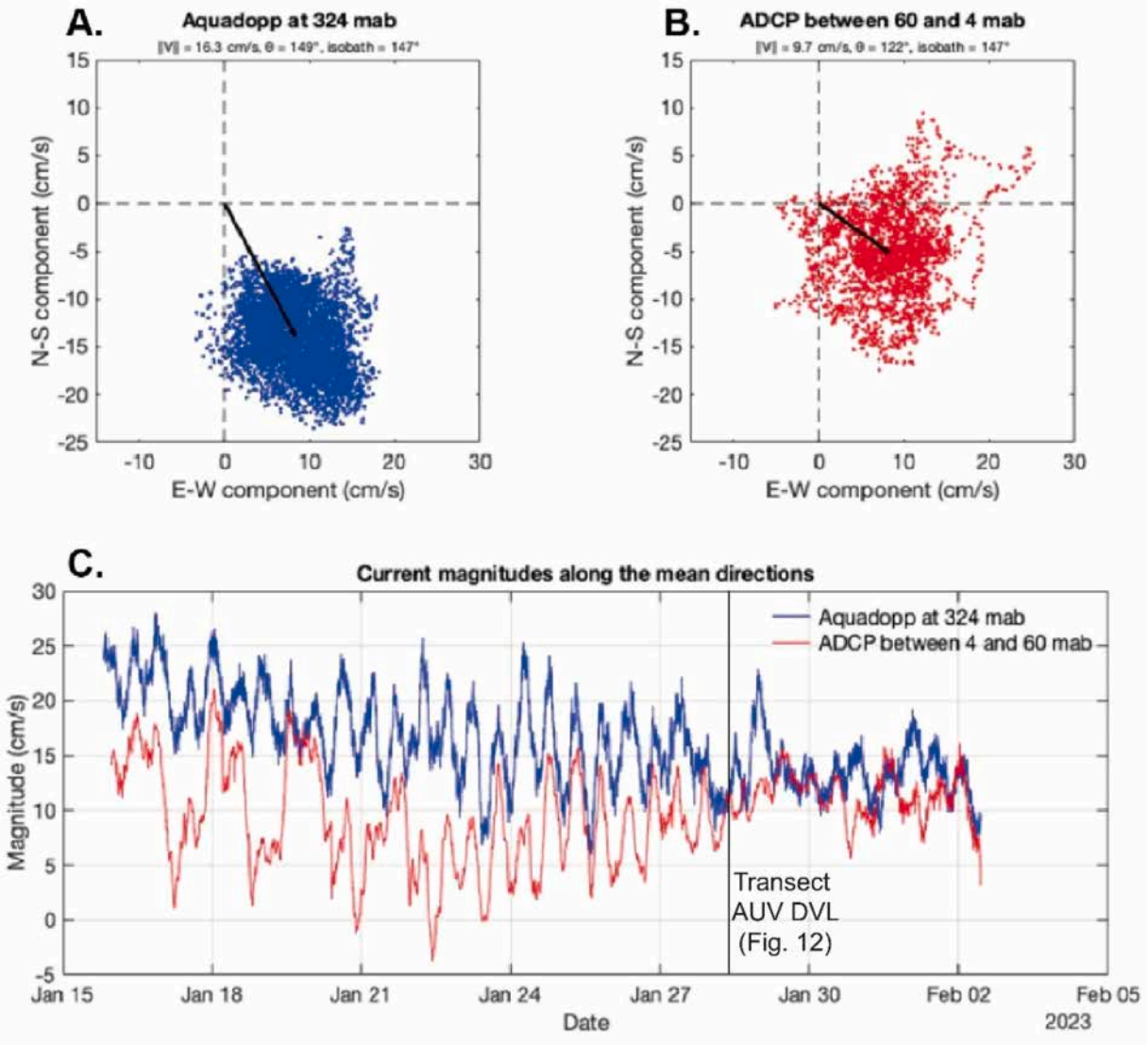

Fig. 11. Current measurements at the mooring site on January 15, 2023 and February 2, 2023 during the DIADEM oceanographic cruise: (a) scatter plots and mean vector of the current measured by the Aquadopp current meter at 320 mab outside the BML (blue), (b) scatterplot and mean vector of the current measured by the ADCP between 4 and 60 mab within the BML. (c) time series of the current component along the mean current directions above (blue) and within (red) the BML. (For interpretation of the references to colour in this figure legend, the reader is referred to the web version of this article.)

lacking sessile organisms, yet display relatively high faunal density (81 individuals per 1000 m^2), mostly Echinoderms. The comet head/crescent scour zone is divided into two subzones, represented in beige and light orange in Fig. 13. The beige subzone encompasses the entire comet head/crescent scour area (7 segments) and exhibits the highest density, averaging 98.4 individuals per 1000 m^2, although taxonomic diversity remains low with 1.4 taxa per 1000 m^2. Despite the low diversity, all major taxa are present, including Arthropods, Cnidarians, Echinoderms, Osteichthyes, Sponges, and Chondrichthyes. This subzone also covers the largest area with a total of 20,403 m^2. The light orange subzone corresponds specifically to the comet head area under the current (2 segments) and covers a smaller area of 2941 m^2. It has a lower density of 24.8 individuals per 1000 m^2, but a higher taxonomic diversity of 2.7 taxa per 1000 m^2, with taxa like the beige subzone but lacking Chondrichthyes. The last zone analyzed is the upstream (2 segments), which covers the smallest area of 1097 m^2. It shows a lower density of 43.7 individuals per 1000 m^2 compare to the comet tail area (other area with sediment cover) but has a much higher normalized taxonomic diversity of 2.7 taxa per 1000 m^2, although only three different species were identified in this zone.

On the metric scale and for two little blocks in the complex area comet's head/crescent scour, the area facing the current supports a significantly higher number of individuals (33 individuals on average) than the area in the lee of the current (5 individuals on average). Although the total number of individuals depends on block size, the proportion remains stable across conditions, with 87% facing the current and 13% oriented downstream (Fig. 13.e, fixed life in indurated outcrops with current coming from the left of the image).

For a more robust relative comparison, the same methodology was applied to two additional sites explored during the DIADEM campaign (Fig. 14).

The first comparison is with NAUT07, located near the study site (see Fig. 7) in Tangara East. This site displays both lower taxonomic diversity and lower density (Fig. 14.a, 14.b). Yet this site exhibits a relatively similar taxonomic assemblage to the study site with a co-occurrence of 59%, based on the Jaccard index (Jaccard, 1901). Furthermore, the two dominant species occur in similar proportions in both sites: *Ophionotus victoriae, Ophiuroidea* (59% at NAUT02 and 54% at NAUT07), *Pachastrella monilifera*, *Demospongiae* (14% in both sites). Finally, a comparison was made with NAUT06, located about 500 m from NAUT02 in the same

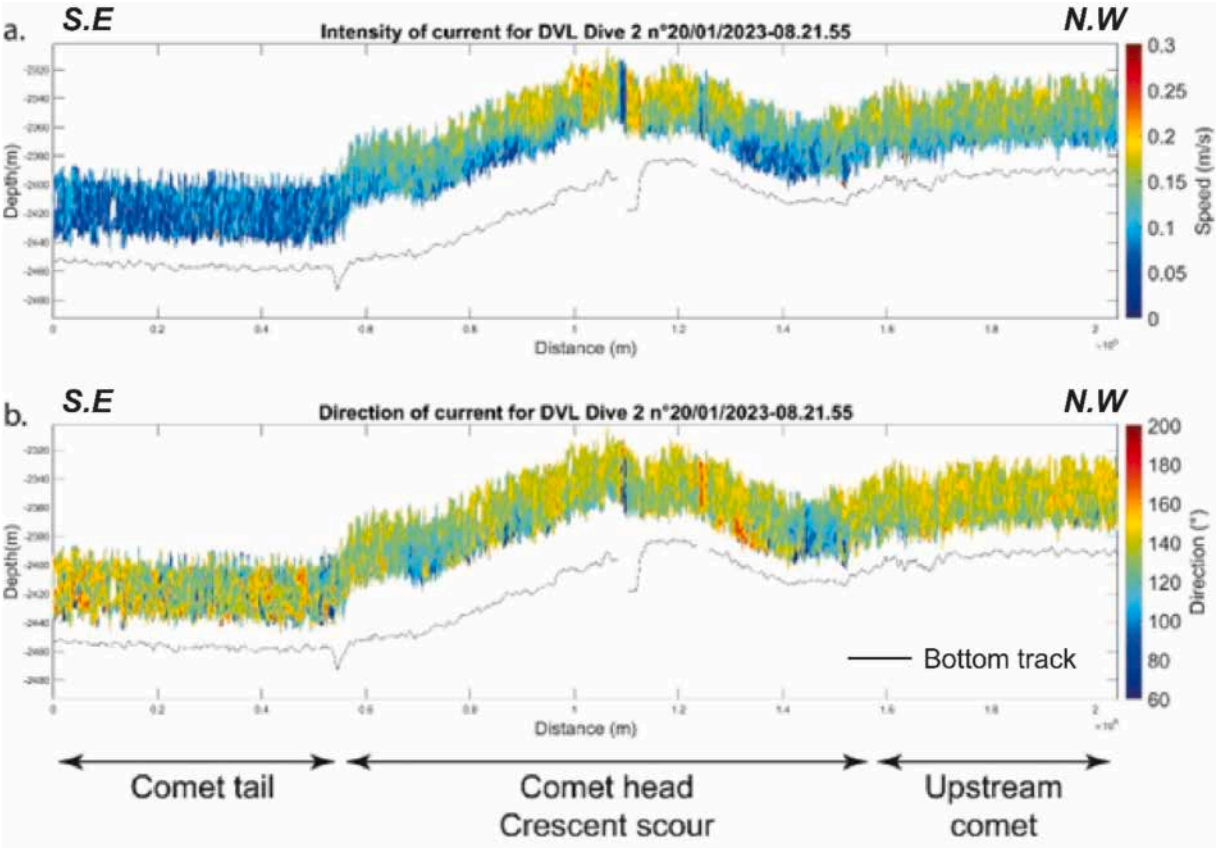

Fig. 12. Profiles of the speed (a) and direction (b) of the current between 70 and 20 mab measured by the AUV along the axis of the main Tangara comet-mark along Dive 2 January 28th, 2023, at 08:21:55 UTC lasting for 23 min (location of DVL survey in Fig. 2) during the peak of the tidal flow. The different parts of the comet (tail, crescent scour, comet head and upstream) are defined.

comet field. This site shows the highest co-occurrence value (62%) with study site (NAUT02) and display the highest taxonomic diversity (1.1 taxa/1000 m^2) with a density very similar to that of the study site. The dominant species are also the same as those recorded at NAUT02, namely *Ophionotus victoriae, Ophiuroidea* (38%), *Pachastrella monilifera, Demospongiae* (23%), and *Pachastrella abyssi, Demospongiae* (8.5%, same as NAUT02).

The values of Shannon and Simpson indices (Colwell, 2009) in NAUT07 are comparable to those of the study area, with differences of only 2% and 7%, respectively. In contrast, NAUT06 displays the highest values for both indices, with differences reaching up to 24% (Fig. 14.c, 14.d).

5. Interpretation and discussion

Several key questions arise from this study and can be grouped into four main discussion topics:

(e.g. 5.1) Does the structure of the indurated comet head originate from fluid seepage through pockmarks and the formation of methane-derived authigenic carbonates (MDAC), from mass transport deposits (MTD), or from coralligenous bioconstructions, these constituting the three main assumptions (Loncke et al., 2016; Pattier et al., 2013a; Tallobre, 2017)?

(e.g. 5.2) Is the system undergoing continuous erosion, or are there other types of dynamic behaviour through time?

(e.g. 5.3) Can giant comet marks be reliably used as geo-currentometers to assess bottom current variability in real-world environments?

(e.g. 5.4) How do sedimentary environments and bedforms along the comet structure influence biodiversity and species abundance?

5.1. Nature of the indurated obstacle at the comet head

Loncke et al. (2016) and Pattier et al. (2013a, 2013b) suspected that methane ascents from depth could have formed some of the depressions behind comet-heads (initially interpreted as pockmarks in Pattier et al., 2013a, 2013b) but also that such methane ascents could be oxidized anaerobically by microbial consortia at the sulphate-methane boundary in the sediments resulting in the precipitation of MDACs (Methane Derived Authigenic Carbonate) on the seafloor (Kravchishina et al., 2021; Sauer et al., 2017). The new data presented here rather show that the comet-like structures observed in this study are linked to a mass transport deposit (MTD) outcropping on the seafloor. This hypothesis is supported by multiple data sets presented here which also excludes the other two hypotheses of MDAC and bioconstruction. The analysis of seismic data reveals an acoustically transparent to chaotic mass dating from the Miocene/Pliocene (Pattier et al., 2013a, 2013b) that thickens (compressive toe, Fig. 4.c) and outcrops on the seafloor in the comet head domain (Fig. 3). Observations from the Nautile submersible highlight the occurrence of carbonate outcrops composed of stratified, white and relatively friable indurated rocks. Those dives also evidenced folds, faults and significant block reworking, together with the chaotic orientation of bedding and variability of dips and azimuth (Fig. 7). In-situ observations combined with petrographic and mineralogical characterization of a rock sampled at the outcrop of the comet heads reveal that the white carbonate strata are composed mainly of biogenic calcite even if a small area of authigenic aragonite was observed, mostly originated from dissolution and reprecipitation processes of biogenic exoskeleton initially formed by this carbonate phase (Fig. 8). This result is in accordance with industrial and ODP (Ocean Drilling Program) wells that record chalky sedimentation in Oligocene to Miocene stratigraphy

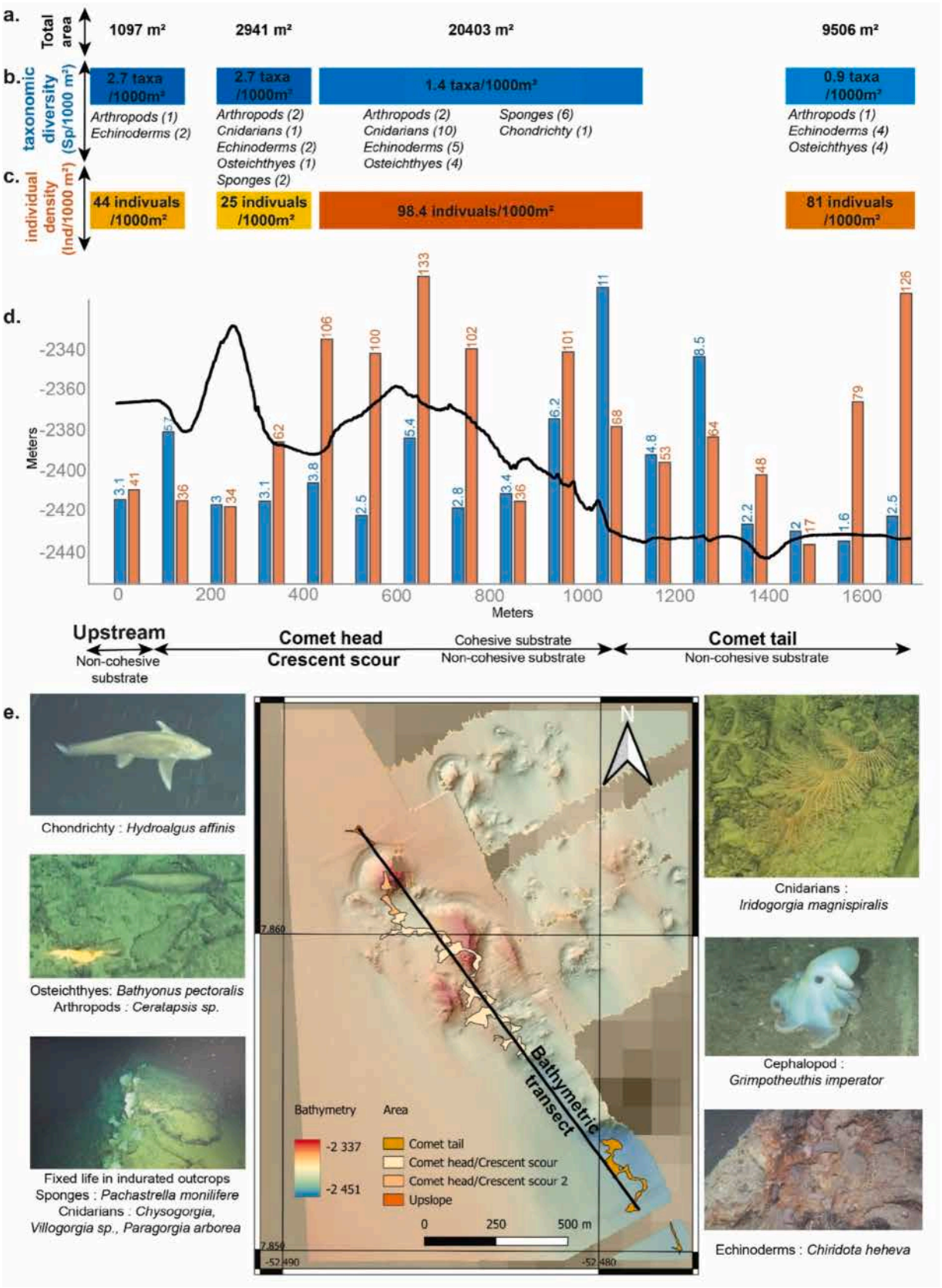

Fig. 13. (a) total area covered by the different subzones studied. (b) Taxonomic diversity (blue): number of different taxa per 1000 m^2 per zone as well as the different taxa found per zone and in brackets the numbers of different taxa per phylum or class. (c) Density of individuals in number of individuals per 1000 m^2 (orange). (d) Bathymetric profile and location of the different 100 m segments showing taxonomic diversity index (blue) and the density per 1000 m^2 for each transect (orange). (e) location on the bathymetric transect of the upstream, the comet head/crescent scour and the comet tail, and Illustrations of the different taxa found along Tangara comet-mark.

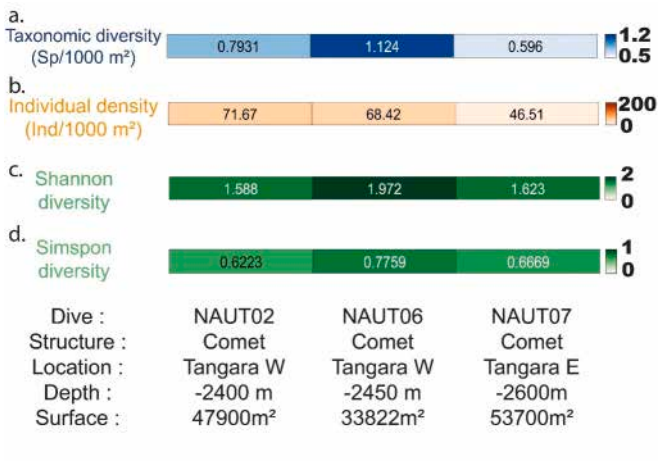

Fig. 14. (a) Taxonomic diversity and (b) density (per 1000 m^2), Shannon diversity index (c), Simspon diversity index (d) at each site.

(Gouyet, 1988). Carbonated MTDs have already been sampled in the past, through coring on the study area located 450 m northwest of the upstream. Sr analysis of those samples suggests an Oligocene to Miocene age of those carbonates, later remobilized (Tallobre, 2017). All these recent and past observations and analysis thus sustain the idea that the indurated rocks forming the obstacles in the NADW flow consist in Oligocene to Miocene carbonates remobilized from the upper slope between the upper Miocene and Lower Pliocene rather than MDACS related to active fluid venting (Pattier et al., 2013a, 2013b). Futhermore, *Chiridota heheva, Holothuroidea* (Fig. 13.e) which are holothurians typically associated with chemosynthetic ecosystems and fluid seeps (Thomas et al., 2020) have been found in several comet-marks outcrops and systematically associated with yellowish-coloured rock. One of those occurrences has been localized on the seismic profile (Fig. 4.d). It locates above the acoustically transparent to chaotic MTD zone, itself emplaced above a highly faulted interval that may be conducting deep fluids to the surface, and along MTD thrust faults that rise to the seafloor. These fluids are originate from the Upper Cretaceous. Immediately after the formation of the Albian unconformity, repeated oceanic anoxic events led to the deposition of organic-rich black shales of Cenomanian-Turonian age on the Demerara Shelf (Friedrich and Erbacher, 2006; Pattier et al., 2013a; Wagner and Pletsch, 1999). These units represent a potential long-term source of fluids generated by organic matter degradation and have been proven laterally on ODP leg 207 (O'Reagan and Moran, 2007) to be the locus of elevated methane concentrations. Due to the various vertical faults originating from this series, it's suspected that some of these highly diffuse seepage fluids have risen to the surface.

5.2. Polyphase evolution of comet-mark structure

High-Resolution seismic data analysis reveals that post-Pliocene sedimentation is characterized by a succession of erosional and depositional phases, resulting in polyphase sedimentation. When main erosion occurs, it is enhanced in the comet-tail domain (see erosion surfaces 01, 02, 03) with a deepening of the erosional surfaces forming giant furrows downstream of the comet-heads. Three main erosional surfaces document 3 major hydrodynamic pulses since the Pliocene. In between those erosional surfaces, sediments infill the comet tail domain with fan-shaped geometries. The last evolutionary stage is clearly depositional at the scale of seismic data (Fig. 4.b). At a finer scale, CHIRP seismic data confirm the depositional nature of the most recent sedimentary layer (Fig. 4.c). The AUV chirp data indicate a zone of deposition in the tail of the comet in the most recent sediments, which is marked by a thickening of the main reflectors towards the comet head. This thickening is attributed to a larger accommodation space following previous erosions. Following phases of erosion induced by accelerated bottom currents, the comet tail exhibits a morphological depression resulting from preferential sediment removal. During subsequent phases of reduced hydrodynamic energy, this depression acts as a localized accommodation space, promoting the trapping and accumulation of fine-grained sediments. Under present-day conditions, characterized by lower current velocities, the comet tail therefore functions as a preferential depositional area. This interpretation is supported by the fan-shaped geometry of the sediment bodies observed within the tail, which reflects the progressive infilling of the accommodation space created during earlier erosional phases.

Fig. 15 presents a simplified model for the evolution of the comet, summarizing the findings of this study and emphasizing the polyphase evolution of this structure. The first phase corresponds to the upper Miocene to lower Pliocene MTD emplacement (Fanget et al., 2020; Pattier et al., 2013a, 2013b; Tallobre, 2017) that consistsof cemented carbonate sediments that thicken on the MTD toe and form obstacles on the seafloor when the modern NADW current establishment. The second phase corresponds to a sedimentary infill controlled by a contourite depositional system associated with the activity of the Deep Western Boundary Current (DWBC). After that, alternating erosion (like in phases 3 & 5) and deposition (like in phases 4 & 6) phases are recorded in the comet-tail domain signing contrasted hydrodynamic conditions through time. Interpretation of the erosion/scouring phases as periods of higher hydrodynamic conditions while fan-shaped deposition phases sign lower current velocity conditions. At present-day, we are thus in a relatively low-velocity phase associated with larger accommodation space and infilling of the comet tail.

On shorter timescales, sediment cores (Fig. 9) support this polyphase evolution, revealing clay-to-silt grain-size successions typical of contouritic systems with alternating deposition, winnowing, and erosion. This small-scale alternation is also supported by the deeper sediment core IG-KS-09 (311 cm) from the IGUANES oceanographic cruise, collected at the tail of the comet-like structure (see location in Figs. 4 and 5), which shows repeated grain-size alternations from clay to silt, characteristic of a contourite depositional system (Tallobre, 2017).

The polyphased development of comet-mark structures is interpreted as a direct response to temporal variations in the intensity of the Deep Western Boundary Current. These variations may reflect successive episodes of acceleration and deceleration, as well as vertical expansion or contraction of the deep-water mass through time. Such hydrodynamic fluctuations would directly control bottom shear stress, sediment erosion, transport, and deposition, thereby driving alternating erosional and depositional phases recorded in the comet-mark morphology.

5.3. Present day hydrodynamics and associated morpho-sedimentary facies

The correlations between the morphological data, hydrodynamical data, and sedimentological characteristics, strongly support the hypothesis that these comet-marks structures are inherited features primarily shaped by more intense paleo-currents. Based on the data presented previously, schematic geographical distribution of the different morpho-sedimentary facies (Fig. 16.a) and the hydrodynamic regimes (Fig. 16.c) are correlated with schematic reflectivity data (Fig. 16.b) collected during the AUV MBES dives across the entire comet structure (crescent scour, comet head and tail). These correlations show that the comet tail is characterized by very fine sediments, which is consistent with low current velocities, and low reflectivity, indicative of a low rugosity, smooth and fine-grained seafloor. In contrast, the crescent scour exhibits stronger currents, coarser sediments with sedimentary features like ripples, and higher reflectivity. Similarly, the comet head shows high reflectivity associated with stronger currents and indurated outcrops devoid of sedimentation on the upstream side.

The hypothesis of a fossil structure is also reinforced by

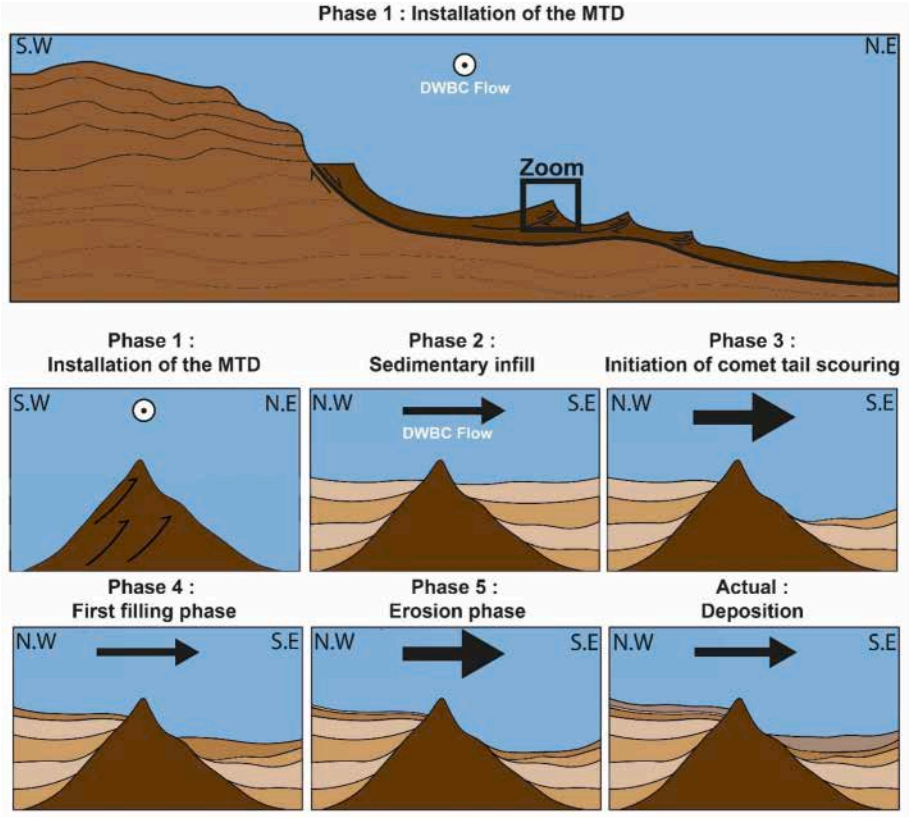

Fig. 15. Scheme presenting a simplified evolution scenario of a comet-mark structure in the study site, emphasizing its polyphase evolution. The thickness of the black arrow varies depending on the intensity of the current.

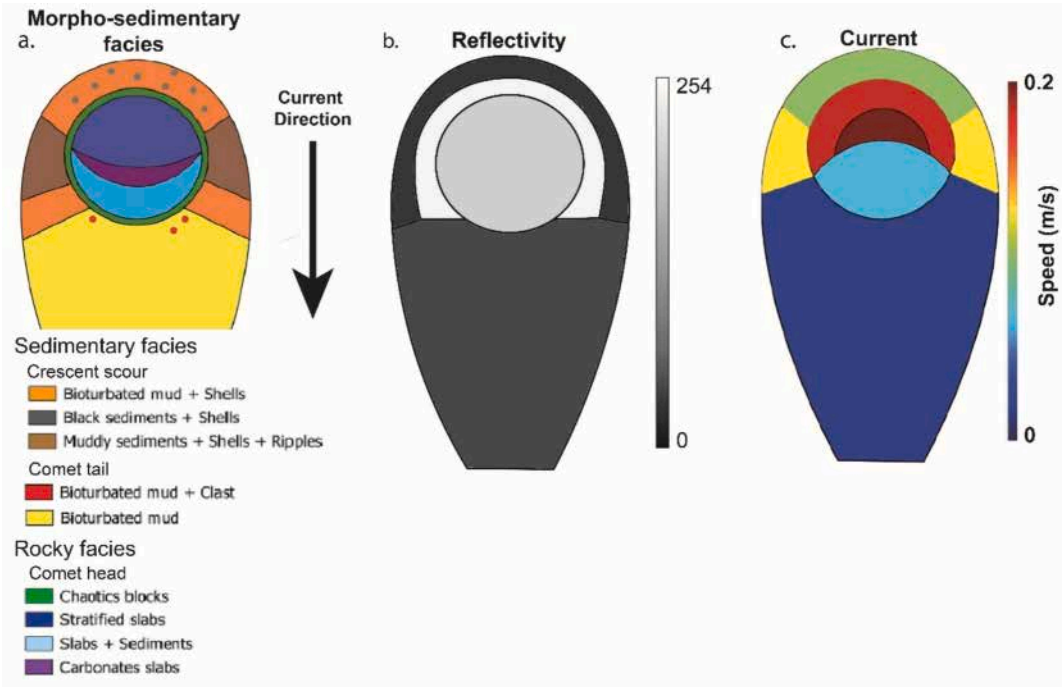

Fig. 16. Schematization of morpho-sedimentary facies data (A), reflectivity data (B) and hydrodynamic data (C).

hydrodynamic data showing low current velocities at the deepest part of the comet tail, with maximum for the last bin (last cell of AUV, approximately 20 m) values below 11 cm/s during high barotropic tides and less than 10 cm/s during low barotropic tides, far from the values necessary for the formation of these structures. According to the Huljstrom diagram taking into account the logarithmic decrease in currents as a function of depth and the sedimentological data from cores DIA23-NAUT02-PC01 and IG-KS-09 from the surface showing a rather clayey

granulometry, this results in a clear zone of deposits in the comet tail on the seabed.

In addition to the primary semidiurnal tidal signal, a secondary oscillation corresponding to the spring and neap tide cycle was also identified from high-frequency ADCP data recorded by the DIADEM mooring. This observation reveals the presence of multiple overlapping temporal scales of hydrodynamic variability, from daily (semidiurnal), to fortnightly (spring-neap), and seasonal. Such variability suggests that, although the present-day current regime is generally weak in the study area, periods of intensified bottom current activity may occur episodically, potentially impacting sediment transport, erosion, and deposition processes compared to the results presented here (period of high seasonal variability, mid-fortnightly tidal variability and high period semidiurnal).

The thickness of the Bottom Mixed Layer (BML) reflects a balance between stratification, Earth's rotation, and near-bottom forcing (Weatherly and Martin, 1978). Deep-ocean stratification is generally weak (Munk and Wunsch, 1998) but tends to intensify near topographic features (Polzin et al., 1997), such as the Demerara Plateau, where stratification values of $N \sim 10^{-3}\ s^{-1}$ are observed.

In the study area, BML thickness is controlled by a combination of hydrodynamic processes that vary both spatially and temporally (Liu et al., 2023). Steady-state Ekman theory, based on a geostrophic bottom flow of approximately 0.16 m/s, predicts a BML thickness of about 70 m. Bottom Ekman dynamics are expected to be persistently active due to the continuous action of geostrophic bottom currents. The resulting Ekman spiral contributes to the redistribution of momentum and sediments near the seabed, maintaining a background level of mixing within the BML. However, this relatively steady process cannot explain the full amplitude of the observed BML thickness variability. Observations instead reveal a much thicker and more variable BML, ranging from <50 to 120 m.

Tidal forcing therefore appears to play a primary role in regulating BML thickness through its interaction with the seabed and the associated enhancement of near-bottom turbulence. During energetic tidal phases, tidal currents increase bottom shear stress, directly contributing to BML thickening. The discrepancy between theoretical predictions and observations is most likely driven by semi-diurnal tidal forcing, which enhances turbulent dissipation and vertical mixing (Liu et al., 2023). Tidal velocity fluctuations of up to ±10 cm/s provide additional energy, allowing turbulence to penetrate significantly further upward against stratification than predicted by steady-state dynamics alone. As a result, BML thickness fluctuates by up to several tens of metres across tidal phases.

Another important point is that the last ADCP pings are recorded at 16 m on average above the seabed, and therefore do not accurately represent shear velocities at the seabed due to the logarithmic decrease in velocity caused by friction (Boudreau and Jørgensen, 2001) at the water-sediment interface.

5.4. Comet-marks as sites of remarkable high biodiversity

The studied comet mark exhibits a remarkable diversity and abundance of benthic and epibenthic species. No previous study specifically addressing the ecological communities associated with such sedimentary structures was found in the literature and this is the first study to provide a detailed description of the ecological communities associated with comet mark sedimentary structures. These findings offer new perspectives for understanding the relationships between hydrodynamic processes, seafloor heterogeneity, and deep-sea biodiversity. The fluid outflow aspect also seems to have an impact on the ecological parameters presented, with a probable impact on the meiofauna as well as the benthic fauna. Firstly, the presence of indurated surfaces promotes the development of sessile organisms. The hypothesis proposed here is that this biological fixation supports the establishment of a more complex trophic network, which could induce higher and more evenly distributed biodiversity. The second point to note is also the large preference of life fixed to the zone facing the current (Fig. 13.e), showing the important role of the indurated surface as well as the contribution of nutrients and oxygen by the DWBC (Wetzel et al., 2008). The variations seem to reflect the influence of environmental factors such as water depth thus specific geomorphological position along the comet-like structures (e.g., head, crescent, or tail).

There are no similar data for comets in the literature. However, comparisons can be made with other structures at similar depths. The density of individuals on hydrothermal vents shows orders of magnitude 10^9 higher, but the diversity of species shows similar values (Marsh et al., 2012). For similar depths in cold environments (Canada Basin) with no bathymetric relief, the orders of magnitude are like slightly equivalent with a factor ranging from *1 to *5 for individual density, However the alpha diversity seems slightly higher on Tangara area (MacDonald et al., 2010). The last comparison on the number of species is made with cold seeps, mud volcanoes and associated slope between 500 and 1412 m in the South China Sea. This study shows a much lower diversity of species with 24 different species in the cold seep zone, 8 for the mud volcanoes and 6 for the continental slope but they don't provide any information about the area covered (Dong et al., 2021). Compared to other studies conducted in deep-sea environments, the diversity observed in our study appears thus high, comparable to that reported from hydrothermal vent ecosystems, and probably higher than that of other deep-sea sites. In contrast, individual abundance is markedly lower.

The relatively high biological diversity observed on comet-mark structures, despite lower individual abundance compared to other deep-sea environments, can be explained by the strong spatial heterogeneity generated by their geological and hydrodynamic characteristics. Comet marks create a complex mosaic of morpho-sedimentary facies over a very limited spatial extent, each associated with distinct sedimentary properties and contrasting hydrodynamic conditions.

This fine-scale heterogeneity promotes the coexistence of multiple ecological niches, allowing benthic species with diverse ecological requirements to colonize preferential micro-environments. In addition, spatial variability in current velocity and direction enhances trophic resource partitioning: areas exposed to stronger currents favour continuous renewal of food supply, whereas sheltered zones promote organic matter accumulation, thereby supporting differentiated trophic strategies. Together, these factors contribute to the high species diversity observed.

Finally, the macrofaunal assemblage presented here is indicative but may be influenced by various biases. This is because the primary focus of these deep-sea investigations was not specifically on macrofauna, and the methodology employed differs from that typically used in studies described in the comparative literature. On the dives presented here, the camera does not have fixed parameters oriented towards the seafloor at a fixed depth, which can lead to distance bias between the number of individuals counted depending on the distance at which they are observed. In addition, the area covered is also much larger in this study, around 50,000 m2 covered compared with 1 to 2500 m^2 for primary research in biology (MacDonald et al., 2010; Marsh et al., 2012). This indicates that this part of the study should be approached with caution, favouring a qualitative interpretation of the results.

6. Conclusions

This multidisciplinary study allows us to draw a new vision of comet-marks structures, environments poorly investigated in the deep sea up to now, and highlights four key findings of either regional or broader interest:

(1) The Demerara plateau is notable for the widespread presence of comet marks covering large areas of the seafloor with kilometre-scale dimensions, and the formation of the indurated comet heads are linked to a mass transport deposit that emplaced between the upper

Miocene and Lower Pliocene, and remobilized older indurated carbonates outcropping now on the seafloor. Those remobilized rocks are suspected to be perturbated by diffuse fluid seepage.

(2) Comet-marks induce topographic steering effects producing a local increase of current velocity above comet-heads but inverse in the comet-tail domain. These highlights evidenced that the investigated comet-tail domain was subjected to low DWBC current velocity at present, undergoing a phase of sediment infilling rather than erosion. The analysis of seismic and sub-bottom profiler data reveals that erosion phases occurred in the past and were responsible for the comet-tail scouring.

(3) This finding refines the interpretation of comet marks as simple indicators of bottom-current intensity. It highlights that these features record a polyphase evolution, driven by temporal variations in bottom-current strength and episodic hydrodynamic events. In addition, the strong vertical velocity gradients near the seabed, induced by friction within the bottom boundary layer, must be considered, as they significantly influence sedimentary processes over several tens to more than one hundred meters above the seafloor in the study area.

(4) The study highlights the impact of these features on benthic and epibenthic biodiversity, revealing a wide variety of associated species that may be promoted by seafloor heterogeneity and roughness but also sediment resuspension.

CRediT authorship contribution statement

Paul Blin: Writing – review & editing, Writing – original draft, Formal analysis. **Lies Loncke:** Writing – review & editing, Supervision, Funding acquisition, Conceptualization. **Xavier Durrieu De Madron:** Writing – review & editing, Supervision, Formal analysis. **Sébastien Zaragosi:** Writing – review & editing, Supervision, Methodology. **Kelly Fauquembergue:** Writing – review & editing. **Swanne Gontharet:** Writing – review & editing, Formal analysis. **Ivane Pairaud:** Writing – review & editing, Methodology. **Pauline Dupont:** Investigation, Formal analysis. **Sandrine Caquineau:** Formal analysis. **Bruno Charriere:** Formal analysis. **Raphael Lagarde:** Writing – review & editing. **Christophe Basile:** Writing – review & editing, Funding acquisition.

Declaration of competing interest

The authors declare that they have no conflict of interest.

The authors declare that they have no known competing financial interests or personal relationships that could have appeared to influence the work reported in this paper.

Acknowledgements

We thank the French Oceanographic Fleet (FOF) for providing access to the research vessels *Pourquoi Pas?* and *L'Atalante*, as well as the equipment used in this study. We are grateful to the crews of the *Pourquoi Pas?* and the scientific team DIADEM for their support during the DIADEM surveys. We also acknowledge the valuable contributions of the Nautile, AUV and sediments core teams for their technical support and information. Special thanks go to Simon Soyez, Pierre Lannes, Cynthia Richard, and Lucie Boitel for their assistance with preliminary data processing.

Data availability

The public datasets are available in the following repertories: IGUANES cruise (doi:10.17600/13010030); and DIADEM cruise (doi:10.17600/18000672). All other supplementary data supporting the findings of this study are available on request from the corresponding author.

References

Augustin, J.-M., 2023. SonarScope Software. https://doi.org/10.17882/87777.
Basile Christophe, 2016. DRADEM cruise, Pourquoi pas ? R/V. https://doi.org/10.17600/16001900.
Basile, C., Loncke, L., 2023. DIADEM cruise, Pourquoi pas ? R/V. https://doi.org/10.17600/18000672.
Basile, C., Maillard, A., Patriat, M., Gaullier, V., Loncke, L., Roest, W., Mercier De Lépinay, M., Pattier, F., 2013. Structure and evolution of the Demerara Plateau, offshore French Guiana: Rifting, tectonic inversion and post-rift tilting at transform–divergent margins intersection. Tectonophysics 591, 16–29. https://doi.org/10.1016/j.tecto.2012.01.010.
Bemis, S.P., Micklethwaite, S., Turner, D., James, M.R., Akciz, S., Thiele, S.T., Bangash, H.A., 2014. Ground-based and UAV-Based photogrammetry: a multi-scale, high-resolution mapping tool for structural geology and paleoseismology. J. Struct. Geol. 69, 163–178. https://doi.org/10.1016/j.jsg.2014.10.007.
Berton, F., Vesely, F.F., 2018. Origin of buried, bottom current-related comet marks and associated submarine bedforms from a Paleogene continental margin, southeastern Brazil. Mar. Geol. 395, 347–362. https://doi.org/10.1016/j.margeo.2017.11.015.
Boudreau, B.P., Jørgensen, B.B. (Eds.), 2001. The Benthic Boundary Layer: Transport Processes and Biogeochemistry. Oxford University Press, Oxford, New York.
Caston, G.F., 1979. Wreck marks: Indicators of net sand transport. Mar. Geol. 33, 193–204. https://doi.org/10.1016/0025-3227(79)90080-X.
Colwell, R.K., 2009. III.1 Biodiversity: Concepts, patterns, and Measurement. In: Levin, S. A., Carpenter, S.R., Godfray, H.C.J., Kinzig, A.P., Loreau, M., Losos, J.B., Walker, B., Wilcove, D.S. (Eds.), The Princeton Guide to Ecology. Princeton University Press, pp. 257–263. https://doi.org/10.1515/9781400833023.257.
Coudun, C., Brichard, P., Basile, C., Zaragosi, S., Marieu, V., Patriat, M., Loncke, L., 2025. Quantitative structural geology in the deep ocean using photogrammetry: Implications for the polyphased tectonic evolution of the Buteur Ridge, French Guiana. Mar. Geol. 488, 107609. https://doi.org/10.1016/j.margeo.2025.107609.
Cushman-Roisin, B., Beckers, J.-M., 2011. The Ekman Layer. In: International Geophysics. Elsevier, pp. 239–270. https://doi.org/10.1016/B978-0-12-088759-0.00008-0.
Dong, D., Li, X., Yang, M., Gong, L., Li, Y., Sui, J., Gan, Z., Kou, Q., Xiao, N., Zhang, J., 2021. Report of epibenthic macrofauna found from Haima cold seeps and adjacent deep-sea habitats, South China Sea. Mar Life Sci Technol 3, 1–12. https://doi.org/10.1007/s42995-020-00073-9.
Dupont, P., Blin, P., 2023. Mission DIADEM : Traitement des données SMF coque et AUV. N/O Pourquoi pas ? 9 Janvier au 7 Février 202 (No. 96689).
Dupont, P., Pacault, A., 2023. Compte rendu d'acquisition des données de sondeur de sédiment. MISSION DIADEM. N/O Pourquoi pas ? 9 Janvier au 7 Février 2022 (No. 96687).
Fanget, A.-S., Loncke, L., Pattier, F., Marsset, T., Roest, W.R., Tallobre, C., Durrieu De Madron, X., Hernández-Molina, F.J., 2020. A synthesis of the sedimentary evolution of the Demerara Plateau (Central Atlantic Ocean) from the late Albian to the Holocene. Mar. Pet. Geol. 114, 104195. https://doi.org/10.1016/j.marpetgeo.2019.104195.
Foglini, F., Campiani, E., Trincardi, F., 2016. The reshaping of the South West Adriatic margin by cascading of dense shelf waters. Mar. Geol. 375, 64–81. https://doi.org/10.1016/j.margeo.2015.08.011.
Friedrich, O., Erbacher, J., 2006. Benthic foraminiferal assemblages from Demerara rise (ODP Leg 207, western tropical Atlantic): possible evidence for a progressive opening of the Equatorial Atlantic Gateway. Cretac. Res. 27, 377–397. https://doi.org/10.1016/j.cretres.2005.07.006.
Gontharet, S., Pierre, C., Blanc-Valleron, M.-M., Rouchy, J.M., Fouquet, Y., Bayon, G., Foucher, J.P., Woodside, J., Mascle, J., 2007. Nature and origin of diagenetic carbonate crusts and concretions from mud volcanoes and pockmarks of the Nile deep-sea fan (eastern Mediterranean Sea). Deep-Sea Res. II Top. Stud. Oceanogr. 54, 1292–1311. https://doi.org/10.1016/j.dsr2.2007.04.007.
Gouyet, S., 1988. Evolution tectono-sédimentaire des marges guyanaise et nord-brésilienne au cours de l'ouverture de l'Atlantique Sud.
Haug, G.H., Tiedemann, R., 1998. Effect of the formation of the Isthmus of Panama on Atlantic Ocean thermohaline circulation. Nature 393, 673–676. https://doi.org/10.1038/31447.
Huang, P., Cen, X., Lu, Y., Guo, S., Zhou, S., 2019. Global distribution of the Oceanic Bottom mixed Layer Thickness. Geophys. Res. Lett. 46, 1547–1554. https://doi.org/10.1029/2018GL081159.
Jaccard, P., 1901. étude Comparative de la distribuition florale dans une portion des Alpes et des Jura. Bull. Soc. Vaudoise Sci. Nat. 7, 547–579.
Kenyon, N.H., 1986. Evidence from bedforms for a strong poleward current along the upper continental slope of Northwest Europe. Mar. Geol. 72, 187–198. https://doi.org/10.1016/0025-3227(86)90106-4.
Klaus Peter Koltermann, V.G, 2011. WOCE Atlas Volume 3: Atlantic Ocean Hydrographic Web Atlas. https://doi.org/10.21976/C6RP4Z.
Kravchishina, M.D., Lein, A.Y., Flint, M.V., Baranov, B.V., Miroshnikov, A.Y., Dubinina, E.O., Dara, O.M., Boev, A.G., Savvichev, A.S., 2021. Methane-Derived Authigenic Carbonates on the Seafloor of the Laptev Sea Shelf. Front. Mar. Sci. 8, 690304. https://doi.org/10.3389/fmars.2021.690304.
Kuijpers, A., Nielsen, T., 2016. Near-bottom current speed maxima in North Atlantic contourite environments inferred from current-induced bedforms and other seabed evidence. Mar. Geol. 378, 230–236. https://doi.org/10.1016/j.margeo.2015.11.003.
Kuijpers, A., Werner, F., Rumohr, J., 1993. Sandwaves and other large-scale bedforms as indicators of non-tidal surge currents in the Skagerrak off Northern Denmark. Mar. Geol. 111, 209–221. https://doi.org/10.1016/0025-3227(93)90131-E.

Kuijpers, A., Hansen, B., Hühnerbach, V., Larsen, B., Nielsen, T., Werner, F., 2002. Norwegian Sea overflow through the Faroe–Shetland gateway as documented by its bedforms. Mar. Geol. 188, 147–164. https://doi.org/10.1016/S0025-3227(02)00279-7.

Le Suave, R., Beuzart, P., 2003. GUYAPLAC cruise, L'Atalante R/V. https://doi.org/10.17600/3010050.

Liu, W., Wang, G., Chen, C., Zhou, M., 2023. Spatial-temporal characteristics of the oceanic bottom mixed layer in the South China Sea. Front. Mar. Sci. 10, 1112535. https://doi.org/10.3389/fmars.2023.1112535.

Loncke Lies, 2013. IGUANES cruise,L'Atalante R/V. https://doi.org/10.17600/13010030.

Loncke, L., Maillard, A., Basile, C., Roest, W.R., Bayon, G., Gaullier, V., Pattier, F., Mercier De Lépinay, M., Grall, C., Droz, L., Marsset, T., Giresse, P., Caprais, J.C., Cathalot, C., Graindorge, D., Heuret, A., Lebrun, J.F., Bermell, S., Marcaillou, B., Sotin, C., Hebert, B., Patriat, M., Bassetti, M.A., Tallobre, C., Buscail, R., Durrieu De Madron, X., Bourrin, F., 2016. Structure of the Demerara passive-transform margin and associated sedimentary processes. Initial results from the IGUANES cruise. SP 431, 179–197. https://doi.org/10.1144/SP431.7.

Loncke, L., Mercier De Lépinay, M., Basile, C., Maillard, A., Roest, W.R., De Clarens, P., Patriat, M., Gaullier, V., Klingelhoefer, F., Graindorge, D., Sapin, F., 2022. Compared structure and evolution of the conjugate Demerara and Guinea transform marginal plateaus. Tectonophysics 822, 229112. https://doi.org/10.1016/j.tecto.2021.229112.

MacDonald, I.R., Bluhm, B.A., Iken, K., Gagaev, S., Strong, S., 2010. Benthic macrofauna and megafauna assemblages in the Arctic deep-sea Canada Basin. Deep-Sea Res. II Top. Stud. Oceanogr. 57, 136–152. https://doi.org/10.1016/j.dsr2.2009.08.012.

Magurran, A.E., 2004. Measuring Biological Diversity. Wiley, S.l.

Marsh, L., Copley, J.T., Huvenne, V.A.I., Linse, K., Reid, W.D.K., Rogers, A.D., Sweeting, C.J., Tyler, P.A., 2012. Microdistribution of Faunal Assemblages at Deep-Sea Hydrothermal Vents in the Southern Ocean. PLoS One 7, e48348. https://doi.org/10.1371/journal.pone.0048348.

Masson, D.G., 2001. Sedimentary processes shaping the eastern slope of the Faeroe–Shetland Channel. Cont. Shelf Res. 21, 825–857. https://doi.org/10.1016/S0278-4343(00)00115-1.

Masson, D.G., Wynn, R.B., Bett, B.J., 2004. Sedimentary environment of the Faroe-Shetland and Faroe Bank Channels, north-East Atlantic, and the use of bedforms as indicators of bottom current velocity in the deep ocean. Sedimentology 51, 1207–1241. https://doi.org/10.1111/j.1365-3091.2004.00668.x.

McDougall, T.J., Barker, P.M., Research, C.M., 2011. Getting Started with TEOS-10 and the Gibbs Seawater (GSW) Oceanographic Toolbox. Trevor J, McDougall.

Munk, W., Wunsch, C., 1998. Abyssal recipes II: energetics of tidal and wind mixing. Deep-Sea Res. I Oceanogr. Res. Pap. 45, 1977–2010. https://doi.org/10.1016/S0967-0637(98)00070-3.

O'Reagan, M., Moran, K., 2007. 15. Compressibility, permeability, and stress history of sediments from Demerara rise, in: Mosher, DC; Erbacher, J; Malone, MJ (eds.) Proceedings of the Ocean Drilling Program.

Pairaud, I., Fuchs, R., 2021. Rapport des campagnes TURBIDENT Leg1 (Mai 2018) & Leg2 (Octobre 2018). Ifremer. https://doi.org/10.13155/78596.

Pattier, F., Loncke, L., Gaullier, V., Basile, C., Maillard, A., Imbert, P., Roest, W.R., Vendeville, B.C., Patriat, M., Loubrieu, B., 2013a. Mass-transport deposits and fluid venting in a transform margin setting, the eastern Demerara Plateau (French Guiana). Mar. Pet. Geol. 46, 287–303. https://doi.org/10.1016/j.marpetgeo.2013.06.010.

Pattier, F., Loncke, L., Gaullier, V., Basile, C., Maillard, A., Imbert, P., Roest, W.R., Vendeville, B.C., Patriat, M., Loubrieu, B., 2013b. Mass-transport deposits and fluid venting in a transform margin setting, the eastern Demerara Plateau (French Guiana). Mar. Pet. Geol. 46, 287–303. https://doi.org/10.1016/j.marpetgeo.2013.06.010.

Pattier, F., Loncke, L., Imbert, P., Gaullier, V., Basile, C., Maillard, A., Roest, W.R., Patriat, M., Vendeville, B.C., Marsset, T., Bayon, G., Cathalot, C., Caprais, J.C., Bermell, S., Sotin, C., Hebert, B., Mercier De Lépinay, M., Lebrun, J.F., Marcaillou, B., Heuret, A., Droz, L., Graindorge, D., Poetisi, E., Berrenstein, H., 2015. Origin of an enigmatic regional Mio-Pliocene unconformity on the Demerara plateau. Mar. Geol. 365, 21–35. https://doi.org/10.1016/j.margeo.2015.04.001.

Polzin, K.L., Toole, J.M., Ledwell, J.R., Schmitt, R.W., 1997. Spatial Variability of Turbulent Mixing in the Abyssal Ocean. Science 276, 93–96. https://doi.org/10.1126/science.276.5309.93.

Poncelet, C., Billant, G., Corre, M.-P., Saunier, A., 2025. Globe (GLobal Oceanographic Bathymetry Explorer) Software. Doi:10.17882/70460.

Quinn, R., 2006. The role of scour in shipwreck site formation processes and the preservation of wreck-associated scour signatures in the sedimentary record – evidence from seabed and sub-surface data. J. Archaeol. Sci. 33, 1419–1432. https://doi.org/10.1016/j.jas.2006.01.011.

Rebesco, M., Hernández-Molina, F.J., Van Rooij, D., Wåhlin, A., 2014. Contourites and associated sediments controlled by deep-water circulation processes: State-of-the-art and future considerations. Mar. Geol. 352, 111–154. https://doi.org/10.1016/j.margeo.2014.03.011.

Sauer, S., Crémière, A., Knies, J., Lepland, A., Sahy, D., Martma, T., Noble, S.R., Schönenberger, J., Klug, M., Schubert, C.J., 2017. U-Th chronology and formation controls of methane-derived authigenic carbonates from the Hola trough seep area, northern Norway. Chem. Geol. 470, 164–179. https://doi.org/10.1016/j.chemgeo.2017.09.004.

Tallobre, C., 2017. Mise en évidence d'un système de dépôt contouritique et des processus sédimentaires associés sur le plateau de Demerara (marge guyanaise). Université de Perpignan Via Domitia.

Tallobre, C., Loncke, L., Bassetti, M.-A., Giresse, P., Bayon, G., Buscail, R., De Madron, X. D., Bourrin, F., Vanhaesebroucke, M., Sotin, C., 2016. Description of a contourite depositional system on the Demerara Plateau: results from geophysical data and sediment cores. Mar. Geol. 378, 56–73. https://doi.org/10.1016/j.margeo.2016.01.003.

Tallobre, C., Loncke, L., Droz, L., Marsset, T., Uusõue, M., Roest, W.R., Fanget, A.-S., Bassetti, M.-A., Giresse, P., Bayon, G., 2021. Echofacies interpretation of Pleistocene to Holocene contourites on the Demerara Plateau and abyssal plain. Interpretation 9. https://doi.org/10.1190/INT-2020-0159.1. SB49–SB65.

Thomas, E.A., Liu, R., Amon, D., Copley, J.T., Glover, A.G., Helyar, S.J., Olu, K., Wiklund, H., Zhang, H., Sigwart, J.D., 2020. Chiridota heheva—the cosmopolitan holothurian. Mar. Biodivers. 50, 110. https://doi.org/10.1007/s12526-020-01128-x.

Wagner, T., Pletsch, T., 1999. Tectono-sedimentary controls on cretaceous black shale deposition along the opening Equatorial Atlantic Gateway (ODP Leg 159). SP 153, 241–265. https://doi.org/10.1144/GSL.SP.1999.153.01.15.

Weatherly, G.L., Martin, P.J., 1978. On the Structure and Dynamics of the Oceanic Bottom Boundary Layer. J. Phys. Oceanogr. 8, 557–570. https://doi.org/10.1175/1520-0485(1978)008%253C0557:OTSADO%253E2.0.CO;2.

Werner, F., Unsöld, G., Koopmann, B., Stefanon, A., 1980. Field observations and flume experiments on the nature of comet marks. Sediment. Geol. 26, 233–262. https://doi.org/10.1016/0037-0738(80)90013-5.

Wetzel, A., Werner, F., Stow, D.A.V., 2008. Chapter 11 Bioturbation and Biogenic Sedimentary Structures in Contourites. In: Developments in Sedimentology. Elsevier, pp. 183–202. https://doi.org/10.1016/S0070-4571(08)10011-5.

Wynn, R.B., Masson, D.G., 2008. Chapter 15 Sediment Waves and Bedforms. In: Developments in Sedimentology. Elsevier, pp. 289–300. https://doi.org/10.1016/S0070-4571(08)10015-2.